


國立交通大學

電子工程學系 電子研究所碩士班

碩士論文題目

應用非均勻矽鍺奈米線在生物感測器上提升其
靈敏度



Utilizing Non-Homogeneous SiGe Nanowires to
Enhance Sensitivity Obviously in Biosensor

研究生：鄭文魁

指導教授：張國明 博士

桂正楣 博士

中華民國九十八年九月

應用非均勻矽鍺奈米線在生物感測器上提升其
靈敏度

Utilizing Non-Homogeneous SiGe Nanowires to
Enhance Sensitivity Obviously in Biosensor

研 究 生：鄭文魁

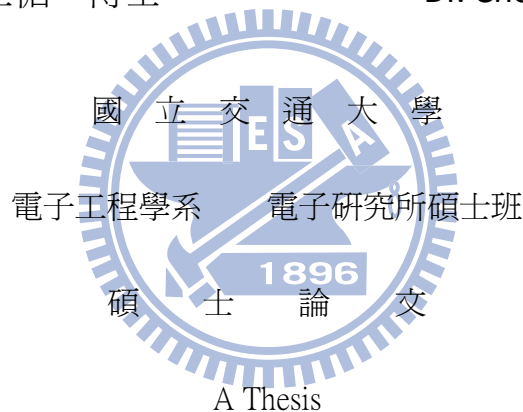
Student : Wen-Kuei Cheng

指導教授：張國明 博士

Advisor : Dr. Kow-Ming Chang

桂正楣 博士

Dr. Cheng-Mei Kuei



Submitted to Department of Electronics Engineering & Institute of Electronics College of
Electrical and Computer Engineering
National Chiao Tung University
In Partial Fulfillment of the Requirements
For the Degree of
Master
In
Electronics Engineering

September 2008, Hsinchu, Taiwan, Republic of China

中華民國九十八年九月

應用非均勻矽鍺奈米線在生物感測器上提升其 靈敏度

研究生：鄭文魁

指導教授：張國明 博士

桂正楣 博士

國立交通大學

電子工程學系 電子研究所碩士班



近年來矽奈米線已被廣泛的應用在生物、化學感測方面。相較於其它感測器，矽奈米線擁有許多優點，例如：矽奈線是即時反應，一旦環境中有待測分子，矽奈米線會立即鍵結住，透過電流變化便可知環境有此分子存在。還有，矽奈米線可偵測濃度非常低的分子，不用透過萃取的方式使濃度增高，便可進行偵測的動作。在此論文中，我們利用半導體製程技術來形成矽鍺奈米線，利用矽鍺氧化鍺析出現象，將鍺析出在奈米線外層，讓矽鍺奈米線形成非均勻，並討論不同的氧化溫度、時間對靈敏度的變化，最後並証實非均勻矽鍺奈米線比均質矽鍺奈米線有較好的感測能力。

Utilizing Non-Homogeneous SiGe Nanowires to Enhance Sensitivity Obviously in Biosensor

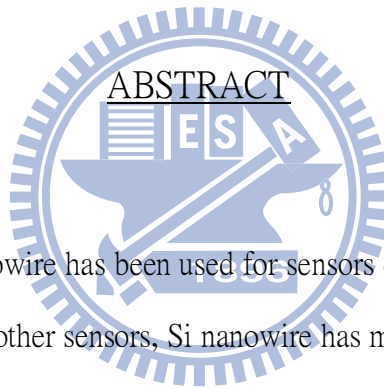
Student : Wen-Kuei Cheng

Advisor : Dr. Kow-Ming Chang

Dr. Cheng-Mei Kuei

Department of Electronics Engineering & Institute of Electronics

National Chiao Tung University , Hsinchu . Taiwan



In recent years , Si nanowire has been used for sensors extensively in biology and chemistry . Comparing with other sensors, Si nanowire has many advantages . For example, Si nanowire is real-time detection, and as soon as the molecule that we want to detect appears in the environment, Si nanowire will bind it. When current change, we can know that the molecule exist in the environment. Moreover, Si nanowires can detect molecule whose concentration can be very low. We don' t need extracting it. In this thesis, we used semiconductor integrated techniques to form SiGe nanowires. Using a Ge condensation technique, Ge will condense on the outer side of nanowire forming non-homogeneous SiGe nanowire, and we discuss different oxidation temperature and time versus sensitivity change. Eventually, we prove that non-homogeneous SiGe had better sensing ability than uniform SiGe nanowire.

誌 謝

首先我要感謝張國明教授和桂正楣教授在這兩年內的指導，讓我在學業上能有所精進，除了學術上的指導，老師時常藉由自己的求學過程來激勵我們，也時常提醒我們當遇到實驗、課程上的問題時要多加思考。除了學業之外，老師也常分享待人處事的道理，對我而言都是相當大的幫助。

其次得感激實驗室的學長、學弟們，尤其是郭俊銘學長、陳巨烽學長、滕聚翔學長、趙文全學長、王育彬同學，劉重顯學弟，感謝大家在學術上對我的指導與實驗上的協助，才使得此論文得以完成。另外也感謝同屆同學們及學弟們，在我心情煩悶時陪伴我，渡過美好的時光。

此外也感謝交大奈米中心、國家奈米元件實驗室(NDL)及其工程師，提供這麼好的實驗機台與人力資源，也感謝交大開課教授們讓我在課堂上學習到寶貴難得的經驗。

最後要感謝我的家人們，感謝家人在背後的支持與鼓勵，才使我碩士能順利畢業，謝謝你們。

誌于 2009. 08

鄭文魁

Contents

| | |
|---|-----|
| Abstract (Chinese) | i |
| Abstract (English) | ii |
| Acknowledgement | iii |
| Contents | iv |
| Figure Captions | vi |
| Chapter 1. Introduction of Nanowire | 1 |
| 1.1 Advantages of nanowire | 1 |
| 1.2 Silicon nanowire is used in chemical detection | 1 |
| 1.2.1 pH detection | 2 |
| 1.2.2 Biotin detection | 2 |
| 1.2.3 DNA detection | 3 |
| 1.2.4 Virus detection | 3 |
| 1.3 Different material of nanowires | 3 |
| 1.3.1 Metal oxide semiconductor nanowire sensors | 4 |
| 1.3.2 Polymer nanowire sensors | 4 |
| 1.3.3 Metal nanowire sensors | 4 |
| 1.4 Silicon nanowire fabrication | 5 |
| 1.4.1 Bottom-up | 5 |
| 1.4.1.1 Silicon nanowire is formed by bottom-up | 5 |
| 1.4.1.2 Si _{1-x} Ge _x nanowire is formed by bottom-up | 5 |
| 1.4.2 Top-down | 6 |
| 1.5 Multiplexed electrical detection | 6 |
| 1.6 Mobility of nanowires | 6 |
| 1.7 Sensing mechanism | 7 |

| | |
|---|----|
| 1.8 Simplified expression of sensitivity | 7 |
| 1.9 Motivation | 8 |
| 1.10 Ge condensation technique | 9 |
| 1.11 Mechanism of SiGe under oxidation | 9 |
| Chapter 2. Experiment | 10 |
| 2.1 Process flow | 10 |
| 2.2 Sensing molecular : APTMS | 11 |
| 2.3 Measurement of electric characteristics | 11 |
| 2.4 Define sensitivity | 12 |
| Chapter 3. 7 percent Ge of SiGe nanowire sensors | 13 |
| 3.1 Cross-section view : 7 percent Ge of SiGe nanowires | 13 |
| 3.2 Defined sensitivity after dipped APTMS | 13 |
| 3.3 Procedure of forming non-homogeneous SiGe nanowire | 13 |
| 3.4 Comparing sensitivity between uniform and non-homogeneous SiGe nanowire. | 14 |
| Chapter 4. 14 percent Ge of SiGe nanowire sensors | 17 |
| 4.1 Cross-section view : 14 percent Ge of SiGe nanowires | 17 |
| 4.2 Defined sensitivity after dipped APTMS | 17 |
| 4.3 Sensitivity is independent of parallel connection number of nanowires | 17 |
| 4.4 Comparing sensitivity between uniform and non-homogeneous SiGe nanowire. | 18 |
| Chapter 5. Conclusions and Future work | 20 |
| References | 44 |

Figure Captions

- Fig. 1-1. (A) Schematic illustrating the conversion of a NWFET into NW pH sensor, (B) Real-time response of an APTES-modified SiNW for pHs from 2 to 9, (C) Plot of the conductance versus pH, and (D) The conductance of unmodified SiNW versus pH (After Y.C. et al, Ref. [1]). 21
- Fig. 1-2. (A) Schematic illustrating a biotin-modified SiNW (left) and subsequent binding of streptavidin to the SiNW surface (right), (B) The conductance increases by positive biotin adsorption. However, the chemical link is irreversible, and (C) The unchanged-conductance is found because of unmodified (After Y.C. et al, Ref. [1]). 22
- Fig. 1-3. Modification scheme of the SiNW surface for the DNA detector:(1) self-assembly of 3-mercaptopropyltrimethoxysilane(MPTMS); (2) covalent immobilization of DNA probes; (3) DNA detection based on hybridization between label-free complementary DNA target and the immobilized DNA probes on the SiNW surfaces (After Z.L. et al, Ref. [2]). 22
- Fig. 1-4. (a) The conductance does not change by un-match DNA (b) Conductance of p-type NW increases after matched-DNA modified (c) Conductance of n-type NW decreases after match-DNA modified (After Z.L. et al, Ref. [2]). 23
- Fig. 1-5. Nanowire-based detection of single virus. (Left) Schematic shows two nanowire devices, 1 and 2, where the nanowires are modified with different antibody receptors. Specific binding of single virus to the receptors on nanowire 2 produce a conductance change (Right) characteristic of the surface change of the virus only in nanowire 2. When the virus unbinds from the surface the conductance return to the baseline value (After F.P. et al, Ref. [3]). 24

Fig. 1-6. Response of the SnO₂ nanobelts to CO at a working temperature of 400 °C and 30% RH (After E.C. et al, Ref. [4]). 24

Fig. 1-7. Measured time-dependent current through an individual CPNM sensor upon exposure to NH₃ gas. The nanowire device being tested was about 335 nm in diameter (After H.L. et al, Ref. [6]). 25

Fig. 1-8. Sensor resistance changes with different H₂ concentration (After K.T.K. et al, Ref. [8]). 25

Fig. 1-9. Schematic illustration: Growth of a silicon crystal by VLS (a) Initial condition with liquid droplet on substrate. (b) Growing crystal with liquid droplet at the tip (After R.S.W. et al, Ref. [10]). 26

Fig. 1-10. SEM images of Si_{1-x}Ge_x nanowires synthesized at different temperatures: (a) 400 °C (b) 430 °C (c) 450 °C (After S.J.W. et al, Ref. [11]). 26

Fig. 1-11. TEM images of Si_{1-x}Ge_x nanowires synthesized at different temperatures: (a) 430 °C (b) 450 °C (After S.J.W. et al, Ref. [11]). 27

Fig. 1-12. Schematic diagram for twin silicon nanowire FET fabrication (After S.D.S. et al, Ref. [12]). 27

Fig. 1-13. Top view and SEM image of nanowire. Diameter is 10 nm and gate length is 30 nm (After S.D.S. et al, Ref. [12]). 27

Fig. 1-14. Cross-section SEM image of nanowire. Nanowire diameter is about 10 nm (After S.D.S. et al, Ref. [12]). 28

Fig. 1-15. Multiplexed electrical detections. NW1 detects PSA; NW2 detects CEA; NW3 detects mucin-1 (After G.Z. et al, Ref. [13]). 28

Fig. 1-16. Schematic of capacitance measurement setup (After R.T. et al, Ref. [15]). 28

Fig. 1-17. Mobility of nanowires is relative to the radius and V_{GS} (After A.C.F. et al, Ref. [14]). 29

| | |
|---|----|
| Fig. 1-18. Nanowire field-effect transistor sensors' sensing mechanism (After F.P. et al, Ref. [19]). | 29 |
| Fig. 1-19. The saturation currents of both short-channel N and P MOSFETs are improved with the use of the SiGe-channel (After Y.C.Y. et al, Ref. [21]). | 29 |
| Fig. 1-20. Procedure for the strained Si on the SGOI structure and Ge profiles (After T.T. et al, Ref. [22]). | 30 |
| Fig. 1-21. TEM image and Ge profile (After T.T. et al, Ref. [22]). | 30 |
| Fig. 2-1. SiO ₂ layer is grown 5000Å on the Si substrate. | 31 |
| Fig. 2-2. Etching SiO ₂ , and the height is about 3000Å. | 31 |
| Fig. 2-3. Depositing α -Si 150Å on the SiO ₂ layer. | 31 |
| Fig. 2-4. Depositing SiGe layer on the amorphous Si layer. | 32 |
| Fig. 2-5. Defined nanowire and S/D. | 32 |
| Fig. 2-6. Etching two side parallel nanowires. | 32 |
| Fig. 2-7. Defined Al contact pad. | 33 |
| Fig. 2-8. APTMS binds silicon oxide layer. | 33 |
| Fig. 3-1. SEM image of Si ₉₃ Ge ₇ nanowire. | 34 |
| Fig. 3-2. I _b -V _D curve of Si ₉₃ Ge ₇ nanowire which is 4µm long before and after dipped APTMS. | 34 |
| Fig. 3-3. Process of forming non-homogeneous SiGe nanowire with three different temperature and post-annealing at 900°C in N ₂ ambient for 30 minutes. | 35 |
| Fig. 3-4. Annealing conditions after oxidation (After C.H.T. et al, Ref. [24]). | 35 |
| Fig. 3-5. Sensitivity distribution of oxidation at 850°C with different time. | 36 |
| Fig. 3-6. Sensitivity distribution of oxidation at 900°C with different time. | 36 |
| Fig. 3-7. Sensitivity distribution of oxidation at 950°C with different time. | 37 |

| | |
|--|----|
| Fig. 3-8. Sensitivity distribution of oxidation time fixed 3 minutes with different oxidation temperatures. | 37 |
| Fig. 3-9. Sensitivity distribution of oxidation time fixed 5 minutes with different oxidation temperatures. | 38 |
| Fig. 3-10. A bar chart of sensitivity distribution with different conditions. | 38 |
| Fig. 4-1. SEM of $\text{Si}_{86}\text{Ge}_{14}$ nanowire. | 39 |
| Fig. 4-2. I_b - V_D curve of $\text{Si}_{86}\text{Ge}_{14}$ nanowire which is 6 μm long before and after dipped APTMS. | 39 |
| Fig. 4-3. Average sensitivity distribution with different parallel connection number of nanowire. | 40 |
| Fig. 4-4. Method of least squares of average sensitivity. | 40 |
| Fig. 4-5. Sensitivity distribution of oxidation at 850°C with different time. | 41 |
| Fig. 4-6. Sensitivity distribution of oxidation at 900°C with different time. | 41 |
| Fig. 4-7. Auger analysis of $\text{Si}_{86}\text{Ge}_{14}$ nanowire without oxidation. | 42 |
| Fig. 4-8. Auger analysis of $\text{Si}_{86}\text{Ge}_{14}$ nanowire at oxidation temperature 900°C for 7 minutes. | 42 |
| Fig. 4-9. Auger analysis of $\text{Si}_{86}\text{Ge}_{14}$ nanowire at oxidation temperature 900°C for 13 minutes. | 43 |
| Fig. 4-10. A bar chart of sensitivity distribution with different conditions. | 43 |

Chapter 1

Introduction of Nanowire

1.1 Advantages of nanowire

In recent years, nanowire has been attracted and used extensively for chemical and biological sensors. Comparing with other sensors, such as ion-sensitive field-effect transistor (ISFET) and chemical field-effect (CHEMFET), silicon nanowire sensor shows a higher sensitivity, faster response, multiplexed electrical detections and higher detection limit, owing to large surface-to-volume. In the other hand, the volume of nanowire is much smaller than planer sensors, in the same chip, which can pack much more nanowire sensors than planer sensors.

There are two main nano sensors. One is nanowire, the other is nanotube. However, several properties of nanotubes would limit their development, including the following:

(1) existing synthetic methods produce mixtures of metallic and semiconducting nanotubes, which make systematic studies difficult because the metallic devices will not function as expected, and (2) flexible methods for the modification of nanotube surfaces, which are required to prepare interfaces selective for binding a wide range of analytes, are not well established [1].

However, nanowire does not have these limitations. Using lithography, we can perform nanowires that we expected, and the doping type and concentration can be controlled easily.

1.2 Silicon nanowire is used in chemical detection

Silicon nanowire is used in chemical detection such as pH buffer solution, protein,

ions, DNA, and virus, etc.

1.2.1 pH detection

Lieber's group presented SiNW pH sensors[1] and investigated the response of SiNWs with and without 3-aminopropyltriethoxysilane(APTES) surface modification. The device structure and the response are shown in Fig. 1-1. The conductance of 3-aminopropyltriethoxysilane-modified SiNWs increased stepwise with discrete changes in pH from 2 to 9 and exhibited a linear pH dependence in Fig. 1-1(B) and 1-1(C). On the other hand, unmodified SiNWs showed nonlinear response in Fig. 1-1(D).

1.2.2 Biotin detection

Not only the pH solution but also other molecules were measured by SiNWs. Fig.1-2(A) shows the diagram after the bio-linker modified and the biotin-streptavidin connected with the bio-linker. Measurements show that the conductance of biotin-modified SiNW increases rapidly to a constant value upon addition of a 250nM streptavidin solution and that this conductance value is maintained after the addition of pure buffer solution Fig. 1-2(B). The increase in conductance upon addition of streptavidin is consistent with binding of a negatively charged species to the p-type SiNW surface and the fact that streptavidin is negatively charged at the pH of our measurements. In addition, several control experiments were carried out to confirm that the observed conductance changes were due to the specific binding of streptavidin to the biotin ligand.

First, addition of a strptavidin solution to an unmodified SiNW did not produce a change in conductance Fig. 1-2(C). Unlike the pH detection, the biotin-streptavidin cannot restore.

1.2.3 DNA detection

DNA detection is a very important thing in biological science and technology. The Sequence-Specific DNA also can be detected by SiNW[2].

The 3-mercaptopropyltrimethoxysilane(MPTMS) by gas-phase reaction in Ar for 4hr was utilized to modify the surface. The CCT-AAT-AAC-AAT DNA linked on it from Fig. 1-3.

The conductance remained the same as the un-match DNA connected, shown in Fig. 1-4(a). However, when SiNW is p-type, the conductance increases as the GGA-TTA-TTG-TTA DNA connect, shown in Fig. 1-4(b). When SiNW is n-type, the conductance decreases as the GGA-TTA-TTG-TTA DNA connect, shown in Fig. 1-4(c).

1.2.4 Virus detection

Viruses are among the most important causes of human disease . We report direct, real-time electrical of single virus particles with high selectivity by using nanowire field effect transistors[3].

Fig. 1-5, when a virus particle binds to the antibody receptor on a nanowire device, the conductance of that device should change from the baseline value, and when the virus unbinds, the conductance should return to the baseline value.

1.3 Different material of nanowires

Nanowire sensors were fabricated by various materials, such as silicon nanowires[1, 2, 3], metal oxide semiconductor nanowire sensors[4, 5, 6], polymer nanowire sensors[6, 7], and metal nanowire sensors[8, 9].

1.3.1 Metal oxide semiconductor nanowire sensors

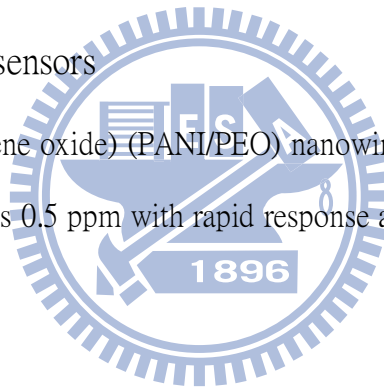
Various kinds of metal oxide nanostructures are reported, including ZnO, SnO₂, In₂O₃, Co₃O₄, CdO, TiO₂, WO₃ and PbO₂, etc. Among these, most attention has been focused on ZnO, SnO₂, and In₂O₃.

For example, Gas sensors have been fabricated using the SnO₂ nanowires[4]. The response of the sensors have been characterized for gas polluting species like CO and NO₂ for environment applications.

Fig. 1-6 shows two different CO concentration 250 and 500 ppm, flowing through the SnO₂ nanowire.

1.3.2 Polymer nanowire sensors

Polyaniline/poly-(ethylene oxide) (PANI/PEO) nanowire sensors that can detect NH₃ gas at concentration as low as 0.5 ppm with rapid response and recovery time as shown in Fig. 1-7.



1.3.3 Metal nanowire sensors

The Hydrogen sensor has been extensively studied for a long time due to safety reasons. Even though several different types of hydrogen sensors utilizing hydrogen-selective Pd metal have been studied, the sensor based on resistance change of Pd nanowires upon hydrogen incorporation has been recently reported and attracted much attention since the sensor has shown extremely low power consumption and very short response time, much less than 1s [8].

The electrical resistance change is dependent on hydrogen concentration, as shown in Fig. 1-8. The more concentration H₂ incorporated in, the higher resistance changed.

1.4 Silicon nanowire fabrication

There are two approaches to form SiNW: bottom-up and top-down.

1.4.1 Bottom-up

1.4.1.1 Silicon nanowire is formed by bottom-up

One of the most approaches for silicon nanowire fabrication is the vapor-liquid-solid (VLS). There are three important facts emerged : (a) silicon whiskers do not contain an axial screw dislocation; (b) an impurity is essential for whisker growth; (c) a small globule is present at the tip of the whisker during growth [10].

A small particle of Au is placed on a {111} surface of a Si wafer and heated to 950 °C, forming a small droplet of Au-Si alloy as shown in Fig. 1-9.

1.4.1.2 Si_{1-x}Ge_x nanowire is formed by bottom-up

The Si_{1-x}Ge_x nanowires have potential advantages of higher carrier mobility and the possible band-gap engineering at different concentration of Ge.

Single crystalline homogeneous Si_{1-x}Ge_x nanowires are synthesized by using monodispersed Au colloids on 100 nm SiO₂ coated Si substrate. SiH₄(100%) and GeH₄ (10% in Ar) gases were simultaneously introduced into a chemical vapor deposition reaction chamber to grow Si_{1-x}Ge_x nanowires. The partial pressure of GeH₄ was kept at 0.12 torr, different temperature by VLS in Fig. 1-10 [11].

Temperature is a very important factor. Fig. 1-11 tells us that Fig. 1-11(a): Point (1) and (2) are little different, but Fig. 1-11(b) [11]: Point (1) and (2) are different.

1.4.2 Top-down

Top-down approaches involve lithography patterning and etching process. Most of the VLSI techniques belong to this category because parameters are much easier controlled than VLS.

Fig. 1-12 showed that used top-down approach to form twin nanowire on Si wafer.

Top view and SEM image of nanowire. Diameter is 10 nm and gate length is 30 nm, shown in Fig. 1-13.

Cross-section SEM image of nanowire. Nanowire diameter is about 10 nm, as shown in Fig. 1-14 [12].

1.5 Multiplexed electrical detections

Many sensors only can detect one molecule in one chip, but nanowire can detect many different molecules in one chip. Fig. 1-15, shows that nanowires can detect three different molecular [13].

1.6 Mobility of nanowires

Mobility is a important factor in the MOSFET, so we also investigate mobility of nanowires. The formula of mobility: $\mu = g_m \frac{L^2}{C_{ox} V_{DS}}$, where $g_m = \frac{dI_{DS}}{dV_{GS}} | V_{DS}$, L is length of nanowire, Cox is capacitance between Gate and Source or Drain [14].

There are two methods to get Cox. One is direct measure, the other is regarding NW as a cylindrical wire on a planar substrate.

Method 1: Direct measure: Fig. 1-16, shows capacitance measurement setup. A

grounded copper plate is positioned between the S/D and G probe tips [15].

Method 2: Regarding NW as a cylindrical wire: The formula is that $C_{ox} = \frac{2\pi\epsilon\epsilon_0L}{\cosh^{-1}[(r+t_{ox})/r]}$ [16-18], where r is radius of nanowire, t_{ox} is the thickness of oxide layer, L is length of nanowire, ϵ is the dielectric constant of the insulator and ϵ_0 is the permittivity of free space.

Fig.1-17 shows that mobility of nanowire is relative to the nanowires' radius and V_{GS} . The reason can be attributed to the surface scattering. When in the high gate voltage or smaller radius, carriers get more scattering, so mobility gets decay [14].

1.7 Sensing mechanism

Nanowire field-effect transistor sensors' sensing mechanism is like MOSFET. When the molecular carry positive charge, for p-type nanowire, it is depletion and then the conductance decreased; when the molecular carry negative charge, for n-type nanowire, it is accumulation, and then the conductance increased, as shown in Fig.1-18 [19].

1.8 Simplified expression of sensitivity

The sensitivity S of a Si-NW sensor is defined as the relative change in conductance, $S = |G - G_0|/G_0 = \Delta G/G_0$, where G_0 is the conductance before molecule capture; G is the conductance after molecule capture and ΔG is the difference between G and G_0 . It is instructive to consider a simplified expression for sensitivity that has been historically used to qualitatively explain sensor response. A series of equations as following [20]:

$$G_0 = q \mu N_D \pi d^2 / 4L_{NW} \quad (1.1)$$

$$\Delta G = \pi \mu \sigma d / L_{NW} \quad (1.2)$$

$$S = \frac{|\Delta G|}{G_0} = \frac{4\sigma}{qdN_D} \quad (1.3)$$

, where d is diameter of nanowire, μ is the mobility of the carriers, N_D is uniform doping density, L_{NW} is length of nanowire, σ is the molecule conjugation on the surface by a constant surface density.

Via Eq. (1.3), we can say that sensitivity is inversely proportional to the diameter. It is same as surface to volume ratio, in other words, and we can say that sensitivity is proportional to the surface-to-volume ratio.

1.9 Motivation

For the study of SiGe field effect transistor, we can find both n-type and p-type MOSFET of SiGe channel, whose current are higher than Si channel, when they are in the same drain voltage, shown in Fig. 1-19 [21]. This mechanism for the silicon nanowire sensor is detecting the surface charges as the molecular stays on it. This result point out SiGe maybe have higher change in electrical property at the same chemical species bonding to surface of nanowires. Therefore, if we used the SiGe nanowire, we would get higher current change at the same bio-molecular bound on the surface.

Moreover, to improve sensitivity, we propose a non-homogeneous structure. The outer layer of nanowire is high conductance, and inner layer is low conductance. Thus, the most current flows through the outer layer, and less current flows through the inner layer. It is like nanotube structure. Nanotube is higher sensitivity than nanowire, because nanotube is hollow, which the surface-to-volume ratio is larger than nanowire. Thus, sensitivity of non-homogeneous is better than that of uniform.

1.10 Ge condensation technique

Oxidation SiGe is named Ge condensation technique. When oxidizing SiGe simultaneously, only Si oxidizes, and Ge concentration gets more and more. We can use this way to let the outer nanowire with high Ge distribution.

In the experiment [22], the wafer is oxidized in O₂ atmosphere at a temperature higher than 1000°C. Via Fig. 1-20 and Fig. 1-21, we can clearly know that oxidation process makes Ge concentration promote on the SiGe layer [22].

1.11 Mechanism of SiGe under oxidation

When oxidizing SiGe simultaneously, Si becomes Si oxide. However, Ge is not oxidized. It is due to their Gibbs free energy difference. Following formulas tell us it [23] :



its Gibbs free energy is $\Delta G_1 = -732 \text{ KJ/mol O}_2$ and



its Gibbs free energy is $\Delta G_2 = -376 \text{ KJ/mol O}_2$. Combing two formulas we can get



its Gibbs free energy is $\Delta G_3 = -356 \text{ KJ/mol O}_2$. It tells us that when SiGe is under oxidation, Si and Ge are both oxidizing. However, when GeO₂ touch Si, GeO₂ return to Ge and Si becomes SiO₂.

Chapter 2

Experiment

In this experiment, we use top-down method to form SiGe nanowires. The method which is very famous is spacer formation to get SiGe nanowires, and then, we take SiGe nanowire undergoing oxidation and annealing at 900°C for 30 minutes in the pure N₂ ambient. Finally, we can get non-homogeneous SiGe nanowires.

2.1 Process flow

Si substrate (100) was used in this study.

1. Standard RCA clean and wet oxidation to grow 5000Å, shown in Fig. 2-1.
2. Mask # 1: Define active area. Using I-line lithography system to transfer pattern to form oxide layer. And then, using TEL 5000 R.I.E dry etching forms step, which is 3000Å high, shown in Fig. 2-2.
3. RCA clean and depositing 150Å α -Si layer, shown in Fig. 2-3.
4. RCA clean and using UHV-CVD depositing SiGe layer, shown in Fig. 2-4.
5. Mask # 2: Define S/D. Using TCP9400 SE poly etcher removes unwanted part and forms parallel nanowires. We have four structures forming many parallel nanowires, respectively forming two, four, six, ten parallel nanowires, so Fig. 2-5, is one among four structures, i.e. this structure forming four parallel nanowires, shown in Fig. 2-5.
6. Mask # 3: Remove unwanted sidewall spacer. TCP poly etcher was employed to remove unwanted spacer, shown in Fig. 2-6.
7. Oxidation in the furnace at different temperature conditions and oxidation time is also a variable condition, and then annealing at 900°C for 30 minutes.

8. Boron-fluoride (BF_2) ion implantation. The implantation dose is 10^{15} ions/cm². Implantation energy is 50 KeV.
9. Oxidation brought about oxide layer in the surface of SiGe nanowire, so using HF etched oxide layer.
10. Annealing in the furnace at 900°C for 30 minutes to activate dopants.
11. 5000Å Aluminum deposition by E-GUN.
12. Mask # 4: Define aluminum contact pad, shown in Fig. 2-7. Using $\text{HNO}_3 : \text{CH}_3\text{COOH} : \text{H}_3\text{PO}_4 : \text{H}_2\text{O} = 2 : 9 : 50 : 10$ mixture etch Al.
13. Al sintering at 400°C in N_2 ambient for 30 minutes.

2.2 Sensing molecular : APTMS

Amino-propyl-trimethoxy-silane (APTMS) is prone to be positively charged. In this experiment, the SiGe nanowire is doped BF_2 forming p-type. When APTMS binds the surface of nanowire's native oxide layer, which is shown as Fig. 2-8, the nanowire will be depletion, and then the current decreases. We can observe the current change and know that APTMS have bound the surface of native oxide layer.

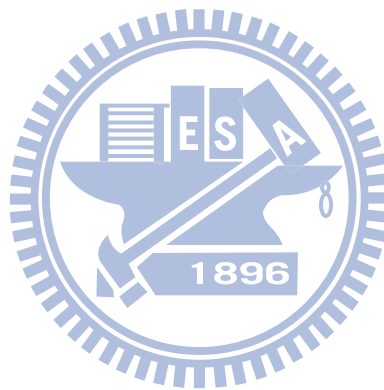
2.3 Measurement of electric characteristics

We used HP4156 to measure the electric characteristics of nanowire sensors. Drain voltage (V_D) was given from -8V to 8V and 200mV a step, and back gate voltage (V_G) was given zero voltage.

2.4 Define sensitivity

In this study, we define sensitivity is that : $S = | I - I_0 | / I_0$, where I_0 is the current of $V_D = -8V$, when nanowire has not dipped APTMS yet; I is the current of $V_D = -8V$, when nanowire has dipped APTMS.

This method is as same as : $S = | G - G_0 | / G_0$ (chapter 1.8), because I_D - V_D curve is a line.



Chapter 3

7 percent Ge of SiGe nanowire sensors

3.1 Cross-section view : 7 percent Ge of SiGe nanowires

Si₉₃Ge₇ nanowires were successfully fabricated by sidewall spacer formation. Fig. 3-1 is the SEM images of Si₉₃Ge₇. The height is about 128 nm and the width is about 62 nm. The Si₉₃Ge₇ nanowire is p-type which is doped BF₂, 10¹⁵ ions/cm² and implantation energy is 50 KeV.

3.2 Defined sensitivity after dipped APTMS

We select that the current at V_D = -8V is a baseline. For instance, the length of Si₉₃Ge₇ nanowire is 4μm. Before dipped APTMS, the current is -154.2μA at V_D= -8V; after dipped APTMS, the current change to -141.48μA. Therefore, sensitivity is :

$$S = \left| \frac{(-141.48\mu A) - (-154.2\mu A)}{(-154.2\mu A)} \right| = 8.249\% , \text{ shown in Fig. 3-2.}$$

3.3 Procedure of forming non-homogeneous SiGe nanowire

For performing non-homogeneous SiGe nanowire, We utilize Ge condensation technique to make the outer layer with high Ge distribution. As a result, the outer layer is high conductance. Thus, we can get non-homogeneous structure.

First, we oxidize Si₉₃Ge₇ nanowire with three different temperatures (850°C, 900°C and 950°C) and post-annealing in pure N₂ ambient at 900°C for 30 minutes. The procedure chart show in Fig. 3-3.

The aim of annealing is that it can repair defects after oxidation. One of pre-work is annealing condition in our group. Fig. 3-4, shows that annealing at 900°C for 30 minutes gets better conductance change, so we still follow this condition [24].

In this experiment, we perform three different oxidation temperatures with different oxidation time, and discussing the effect of temperature and time on the sensitivity.

3.4 Comparing sensitivity between uniform and non-homogeneous SiGe nanowire

Box chart, Fig. 3-5, shows oxidizing $\text{Si}_{93}\text{Ge}_7$ nanowire at 850°C for 0, 3 and 5 minutes. Box chart in the middle has a quadrangle. If there are a group data, the 75 percent value from little to large means the upper line of the box chart, and the 50 percent and 25 percent value mean the middle and lower line of the box chart, respectively. The point in the middle quadrangle means the group data's mean value.

Via Fig. 3-5, the mean value is 7.8119% without oxidation. After oxidation at 850°C for 3 minutes, the mean value is 8.7493%. Moreover, oxidation at 850°C for 5 minutes, the mean value is 9.6674%. The trend is that sensitivity promote along with oxidation time.

And then, we want to know that temperature affects sensitivity of SiGe nanowire, so we promote oxidation temperature 50°C; that is 900°C.

Fig. 3-6, shows that the mean value is 7.8119% without oxidation. After oxidation at 900°C for 3 minutes, the mean value is 9.7711%. Furthermore, oxidation at 900°C for 5 minutes, the mean value is 12.0689%. Via these results, we also can get the trend. Sensitivity is promoting along with oxidation time at 900°C.

To go on, we add oxidation temperature 50°C again; that is, oxidation temperature fixed at 950°C.

When no oxidizing, the mean sensitivity is 7.8119%, and the mean sensitivity is 13.5381% after oxidation at 950°C for 3 minutes. However oxidation at 950°C for 5 minutes, the mean sensitivity is degrading to 10.4265%, shown in Fig. 3-7.

Although oxidation makes Ge concentration promoting in the surface, it also makes defects. We know that it is two mechanism of oxidation of SiGe. One is Ge concentration piling up in the outer layer, so sensitivity increases. The other is that oxidation makes defects, so sensitivity decreases. When oxidation time at 950°C from 3 to 5 minutes, the sensitivity degrades, we guess that the effect of defects is more dominant than Ge concentration promoting on the outer surface of nanowire.

In this study, we need to control oxidation temperature and time to get balance between defects generation and Ge piling up in the outer layer of nanowire.

Oxidation temperature is also a important factor. When we fix oxidation time for 3 minutes, comparing with three oxidation temperatures which are 850°C, 900°C and 950°C, we gets a trend. Sensitivity promotes along with temperature. It accounts for when oxidation temperature from 850°C to 950°C, Ge concentration is not enough, so the sensitivity is promoting, shown as Fig. 3-8.

To continue, we fixed oxidation temperature for 5 minutes, comparing with three oxidation temperatures which are 850°C, 900°C and 950°C, shown as Fig. 3-9. When oxidation temperature from 850°C to 900°C, sensitivity promotes, because at 900°C Ge piling up in outer layer' s velocity is faster than 850°C. However, oxidation temperature from 900°C to 950°C, sensitivity decreases, and we guess that defects generation at 950°C are more than 900°C.

Via Fig. 3-10, in these conditions, the best condition is oxidation at 950°C for 3 minutes, and the sensitivity is 13.5381%. Comparing with uniform Si₉₃Ge₇ nanowire, whose sensitivity is 7.8119%. Subtracting 7.8119% from 13.5381%, the average sensitivity

enhances 5.7262%.



Chapter 4

14 percent Ge of SiGe nanowire sensors

4.1 Cross-section view : 14 percent Ge of SiGe nanowires

Si₈₆Ge₁₄ nanowires were also successfully fabricated by sidewall spacer formation. Fig. 4-1 is the SEM images of Si₈₆Ge₁₄. The height is about 196 nm and the width is about 80 nm. The Si₉₃Ge₇ nanowire is p-type which is doped BF₂, 10¹⁵ ions/cm² and implantation energy is 50KeV.

4.2 Defined sensitivity after dipped APTMS

We select that the current at V_D = -8V is a baseline. For example, the length of Si₈₆Ge₁₄ nanowire is 6um. Before dipped APTMS, the current is -262.25uA at V_D= -8V; after dipped APTMS, the current change to -249.87uA. Therefore, sensitivity is :

$$S = | [(-249.87\mu\text{A}) - (-262.25\mu\text{A})] / (-262.25\mu\text{A}) | = 4.721\% , \text{ shown in Fig. 4-2.}$$

4.3 Sensitivity is independent of parallel connection number of nanowires

Here, we discuss parallel connection number of nanowires affect sensitivity. Average sensitivity of single 、 double 、 quadruple 、 sextuple and decuple parallel connection number of nanowires is 4.50624% 、 4.65438% 、 4.5232% 、 4.5941% and 4.63955%, respectively, shown as Fig. 4-3.

We can clearly see that the average sensitivity of parallel connection number of nanowires is very close to 4.5%.

Moreover, we take these five average point to do **method of least squares** , shown as Fig. 4-4. The slope of the line is 8.74125×10^{-5} . The value is very small and close to a horizontal line. Intercept on y-axis of this line is 4.5433%, and it tells us that average sensitivity is close to 4.5433%.

4.4 Comparing sensitivity between uniform and non-homogeneous SiGe nanowire

Fig. 4-5, shows that oxidizing $\text{Si}_{86}\text{Ge}_{14}$ nanowire temperature at 850°C with 0, 3, 7 and 13 minutes. When nanowire is without oxidation, the average sensitivity is 4.527%. After oxidation at 850°C for 3 minutes, the average sensitivity is promoting to 6.0546%. Adding oxidation time to 7 minutes, the mean sensitivity is increasing to 7.1483%. To go on, adding oxidation time to 13 minutes. However, the average sensitivity is decreasing to 5.1862%. Oxidation time from 0 to 7 minutes, the Ge concentration in outer layer of nanowire is not enough, resulting in sensitivity increasing along with oxidation time. Nevertheless, oxidation time from 7 to 13 minutes, we guess that defects affect sensitivity mainly; therefore, the average sensitivity decreases.

Adding oxidation temperature to 900°C with 0, 3, 7 and 13 minutes. Without oxidation, the average sensitivity of $\text{Si}_{86}\text{Ge}_{14}$ nanowire is 4.527%. After oxidation at 900°C for 3 minutes, the average sensitivity is promoting to 6.5694%. Continuing oxidation, when oxidation at 900°C for 7 minutes, the average sensitivity is promoting to 9.0962%. However, oxidation at 900°C for 13 minutes, the average sensitivity is degrading to 9.0962%. This trend is as same as above data. From 0 to 7 minutes, average sensitivity

increases along with time, and from 7 to 13 minutes, average sensitivity degrades, shown as Fig. 4-6.

When $\text{Si}_{86}\text{Ge}_{14}$ nanowire is no oxidizing, the Ge concentration distribution to Si ratio is close to 14%, shown in Fig. 4-7. After oxidation at 900°C for 7 minutes, the surface of $\text{Si}_{86}\text{Ge}_{14}$ nanowire, Ge concentration to Si concentration ratio is close to 20%, shown in Fig. 4-8. Moreover, Fig. 4-9 shows that after oxidation at 900°C for 13 minutes, the surface of $\text{Si}_{86}\text{Ge}_{14}$ nanowire, Ge concentration to Si concentration ratio is close to 24%. From Fig. 4-7 to Fig. 4-9, we can clearly know that the Ge concentration is piling up on surface which means outer layer of $\text{Si}_{86}\text{Ge}_{14}$ nanowire along with oxidation time.

Via Fig. 4-5 and Fig. 4-6, we can get that higher temperature makes higher sensitivity from 0 to 7 minutes. Higher temperature provides higher energy, letting Ge is easier piling up in the outer layer of SiGe nanowire than lower temperature.

In these conditions, we can get that the best condition is oxidation at 900°C for 7 minutes, and its sensitivity is 9.0962%. Comparing with no oxidation, $\text{Si}_{86}\text{Ge}_{14}$, whose sensitivity is 4.527%. Subtracting 4.527% from 9.0962%, the average sensitivity enhances 4.5692%, shown in Fig. 4-10.

Chapter 5

Conclusions and Future work

Via Ge condensation technique, we successfully performs non-homogeneous SiGe nanowire. Via a series of experiments, we prove that non-homogeneous SiGe nanowire has better sensitivity than uniform SiGe nanowire.

Nevertheless, when oxidation temperature is too high or oxidation time is too long, the sensitivity will decrease. Molecular weight of Ge and Si is very different, when Ge piles up, the interface between Ge and SiO₂ generates amount of defects. Defects make APTMS binding ability degrading, so sensitivity decreases.

If oxidation temperature or oxidation time is not enough, affecting Ge concentration not sufficient, thus sensitivity decreases, because we cannot confine most current flowing through outer layer of nanowire.

Thus, we need appropriate oxidation temperature and time to get best sensitivity.

No matter how number of parallel connection nanowire is, the sensitivity is very close.

In the future, we can discuss that the defects affect sensitivity. Moreover, we need to investigate the concentration of APTMS versus sensitivity and when we measure I_D-V_D curve, different temperatures affect sensitivity.

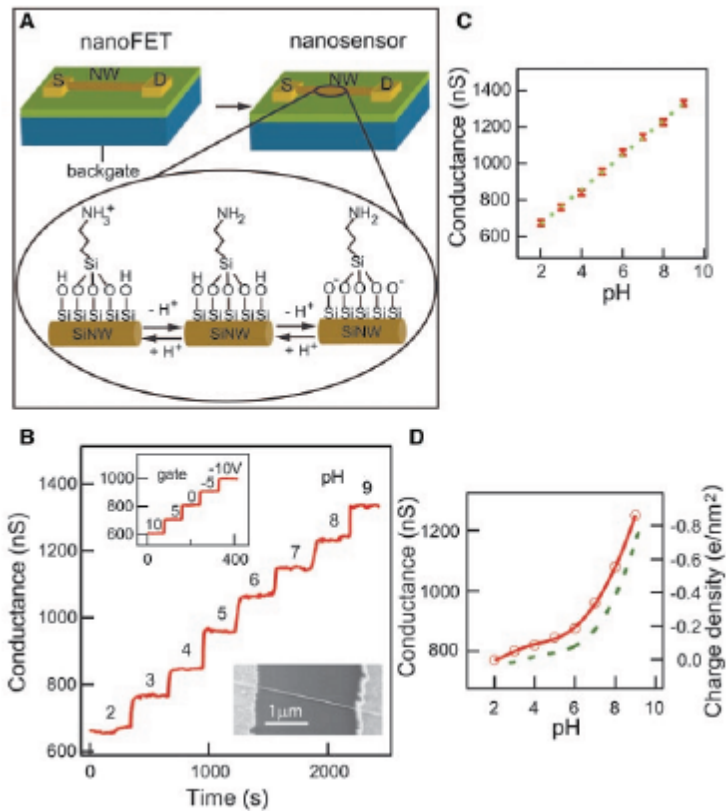


Fig. 1-1. (A) Schematic illustrating the conversion of a NWFET into NW pH sensor, (B) Real-time response of an APTES-modified SiNW for pHs from 2 to 9, (C) Plot of the conductance versus pH, and (D) The conductance of unmodified SiNW versus pH (After Y.C. et al, Ref. [1]).

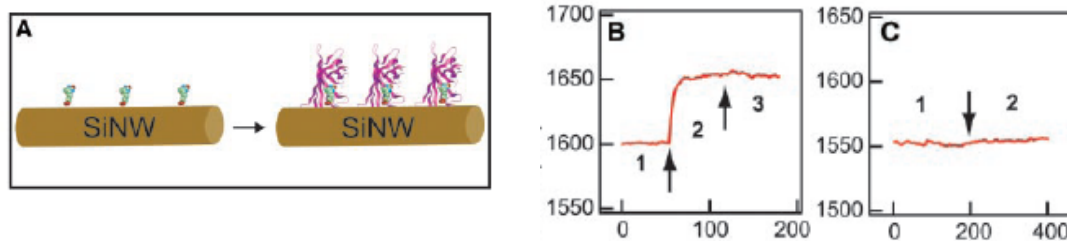


Fig. 1-2. (A) Schematic illustrating a biotin-modified SiNW (left) and subsequent binding of streptavidin to the SiNW surface (right), (B) The conductance increases by positive biotin adsorption. However, the chemical link is irreversible, and (C) The unchanged-conductance is found because of unmodified (After Y.C. et al, Ref. [1]).

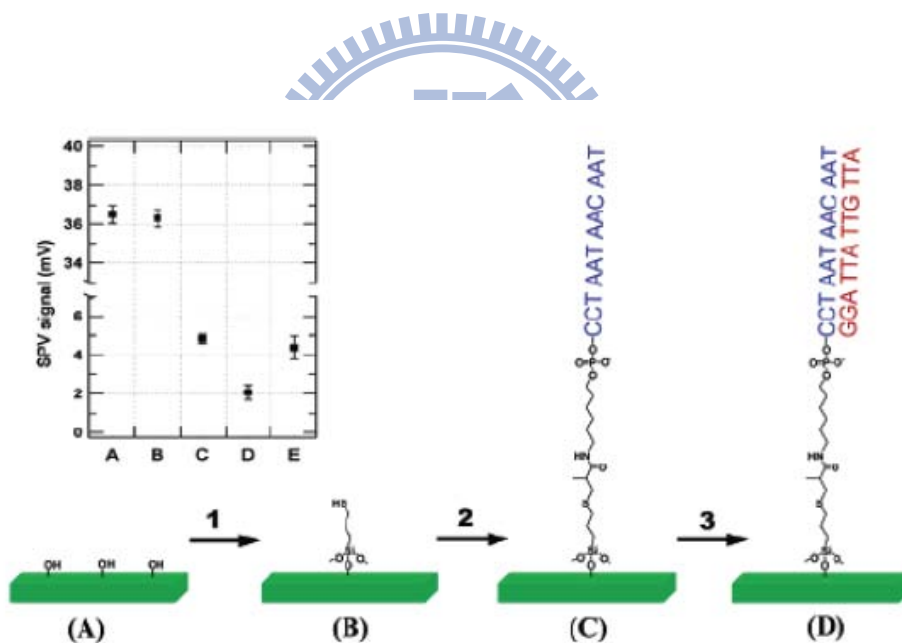


Fig. 1-3. Modification scheme of the SiNW surface for the DNA detector:(1) self-assembly of 3-mercaptopropyltrimethoxysilane(MPTMS); (2) covalent immobilization of DNA probes; (3) DNA detection based on hybridization between label-free complementary DNA target and the immobilized DNA probes on the SiNW surfaces (After Z.L. et al, Ref. [2]).

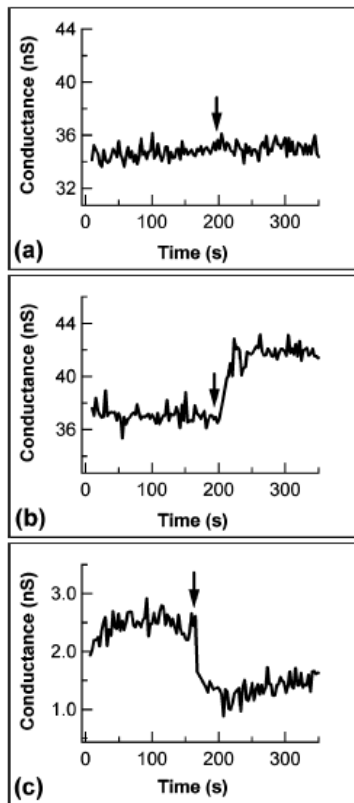


Fig. 1-4. (a) The conductance does not change by un-match DNA (b) Conductance of p-type NW increases after matched-DNA modified (c) Conductance of n-type NW decreases after match-DNA modified (After Z.L. et al, Ref. [2]).

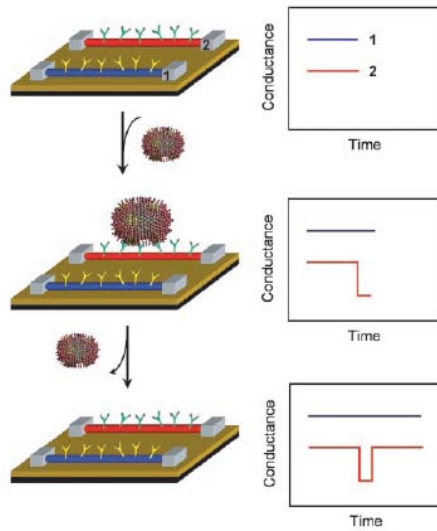


Fig. 1-5. Nanowire-based detection of single virus. (Left) Schematic shows two nanowire devices, 1 and 2, where the nanowires are modified with different antibody receptors. Specific binding of single virus to the receptors on nanowire 2 produce a conductance change (Right) characteristic of the surface change of the virus only in nanowire 2. When the virus unbinds from the surface the conductance return to the baseline value (After F.P. et al, Ref. [3]).

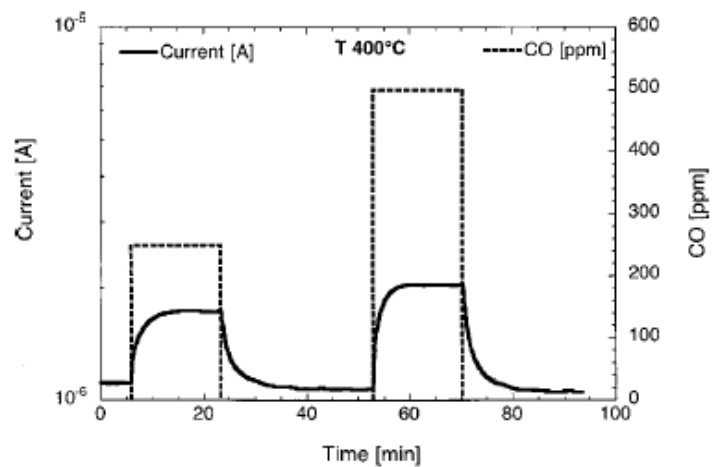


Fig. 1-6. Response of the SnO₂ nanobelts to CO at a working temperature of 400 °C and 30% RH (After E.C. et al, Ref. [4]).

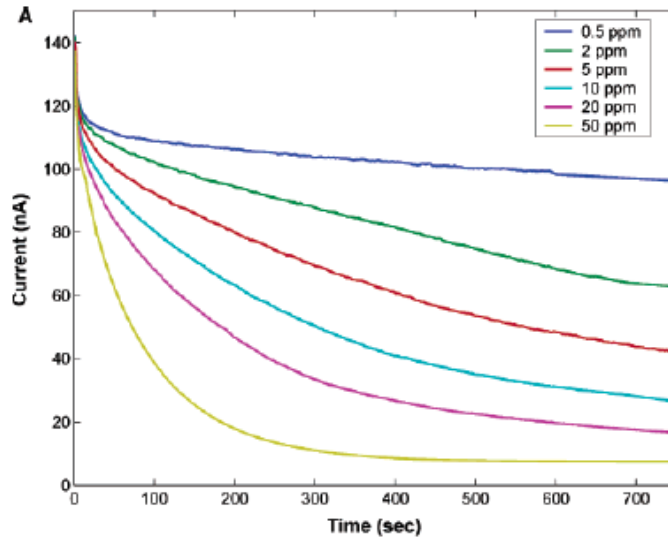


Fig. 1-7. Measured time-dependent current through an individual CPNM sensor upon exposure to NH₃ gas. The nanowire device being tested was about 335 nm in diameter (After H.L. et al, Ref. [6]).

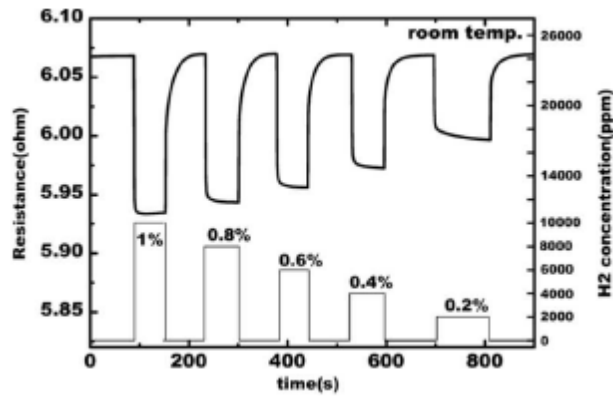
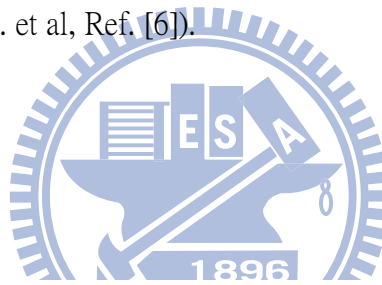


Fig. 1-8. Sensor resistance changes with different H₂ concentration (After K.T.K. et al, Ref. [8]).

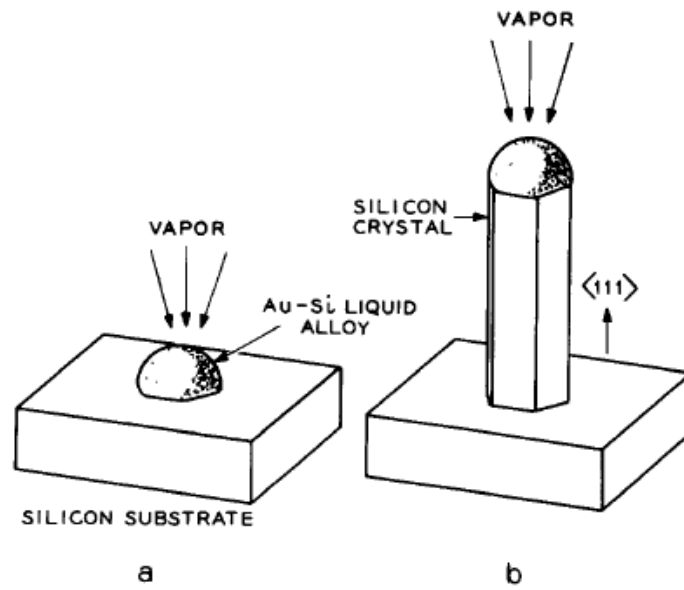


Fig. 1-9. Schematic illustration: Growth of a silicon crystal by VLS (a) Initial condition with liquid droplet on substrate. (b) Growing crystal with liquid droplet at the tip (After R.S.W. et al, Ref. [10]).

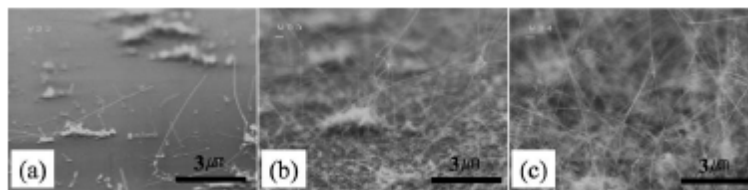


Fig. 1-10. SEM images of $\text{Si}_{1-x}\text{Ge}_x$ nanowires synthesized at different temperatures: (a) 400 °C (b) 430 °C (c) 450 °C (After S.J.W. et al, Ref. [11]).

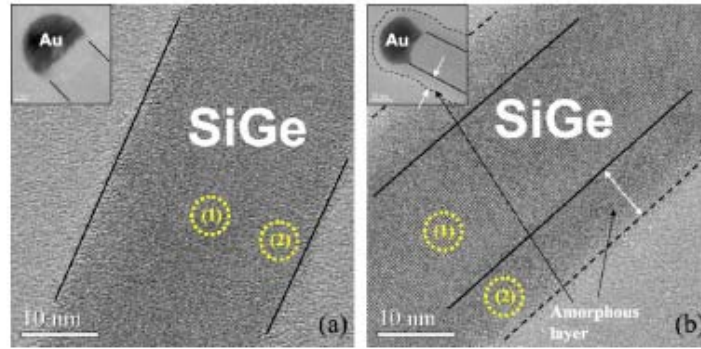


Fig. 1-11. TEM images of $\text{Si}_{1-x}\text{Ge}_x$ nanowires synthesized at different temperatures: (a) 430 °C (b) 450 °C (After S.J.W. et al, Ref. [11]).

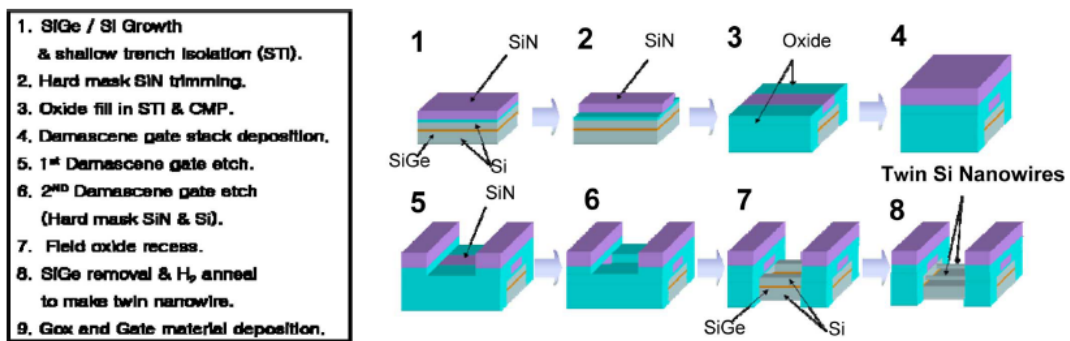


Fig. 1-12. Schematic diagram for twin silicon nanowire FET fabrication (After S.D.S. et al, Ref. [12]).

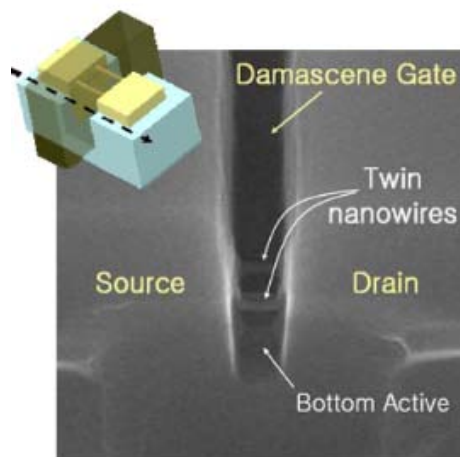


Fig. 1-13. Top view and SEM image of nanowire. Diameter is 10 nm and gate length is 30 nm (After S.D.S. et al, Ref. [12]).

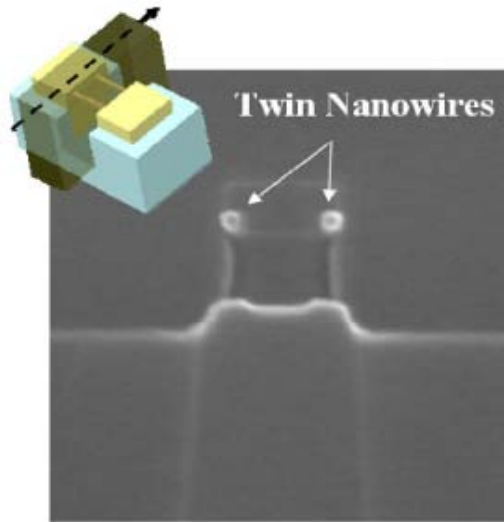


Fig. 1-14. Cross-section SEM image of nanowire. Nanowire diameter is about 10 nm

(After S.D.S. et al, Ref. [12]).

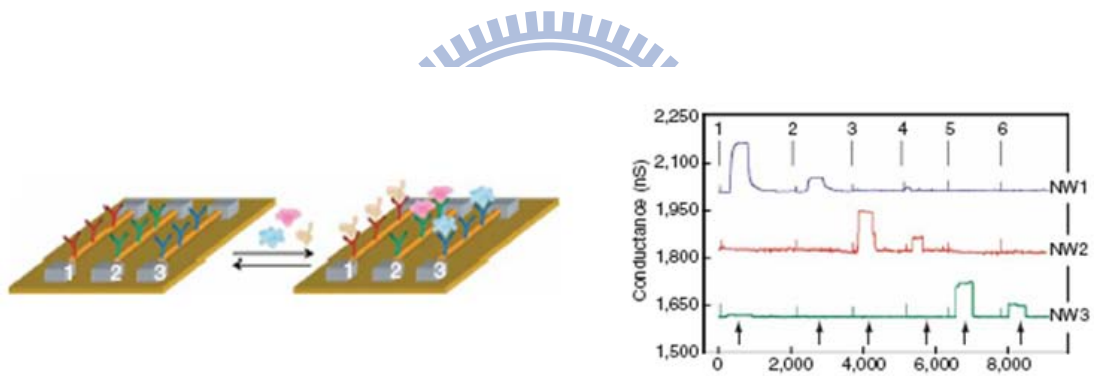


Fig. 1-15. Multiplexed electrical detections. NW1 detects PSA; NW2 detects CEA; NW3

detects mucin-1 (After G.Z. et al, Ref. [13]).

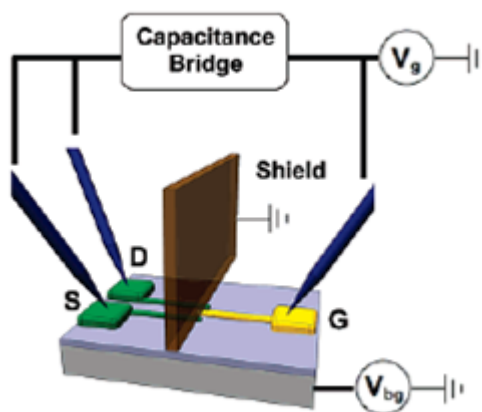


Fig. 1-16. Schematic of capacitance measurement setup (After R.T. et al, Ref. [15]).

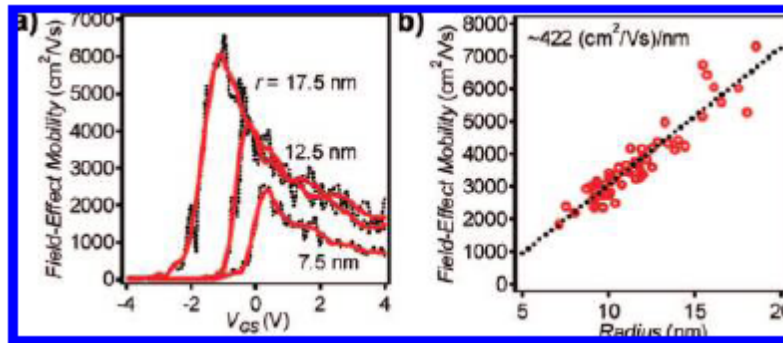


Fig. 1-17. Mobility of nanowires is relative to the radius and V_{GS} (After A.C.F. et al, Ref.

[14]).

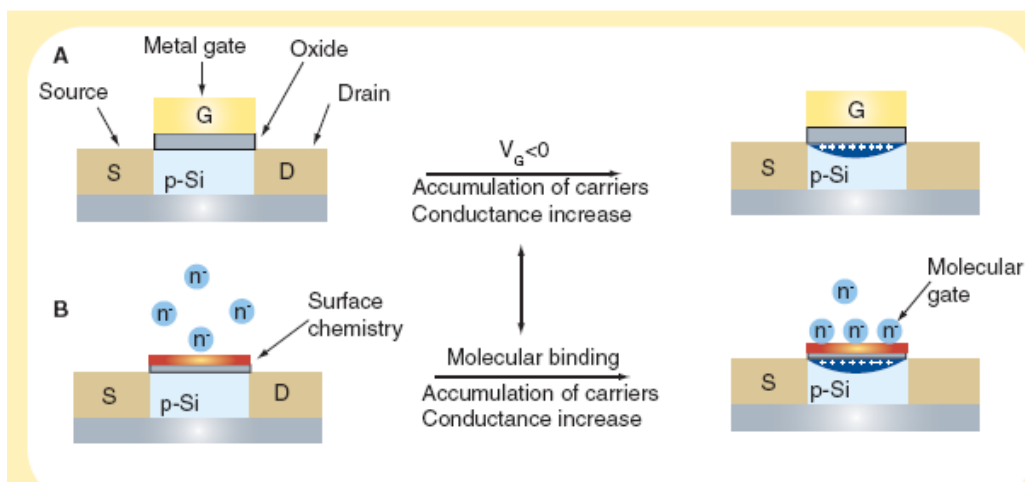


Fig. 1-18. Nanowire field-effect transistor sensors' sensing mechanism (After F.P. et al, Ref. [19]).

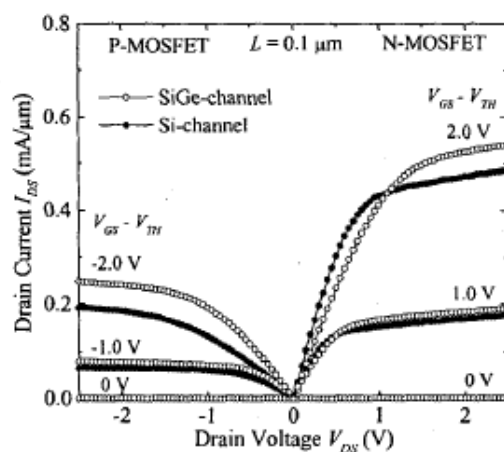


Fig. 1-19. The saturation currents of both short-channel N and P MOSFETs are improved with the use of the SiGe-channel (After Y.C.Y. et al, Ref. [21]).

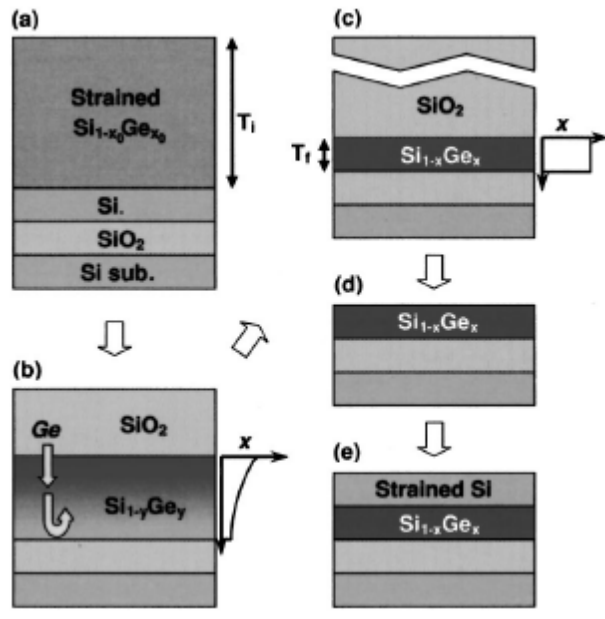


Fig. 1-20. Procedure for the strained Si on the SGOI structure and Ge profiles (After T.T. et al, Ref. [22]).

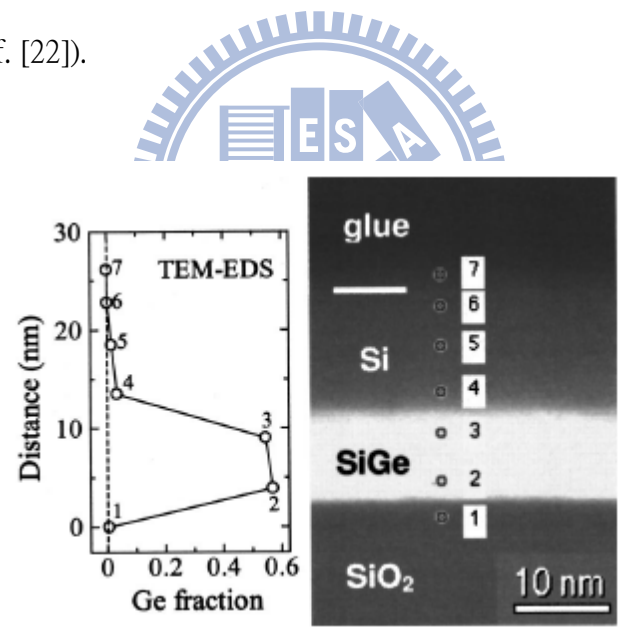


Fig. 1-21. TEM image and Ge profile (After T.T. et al, Ref. [22]).

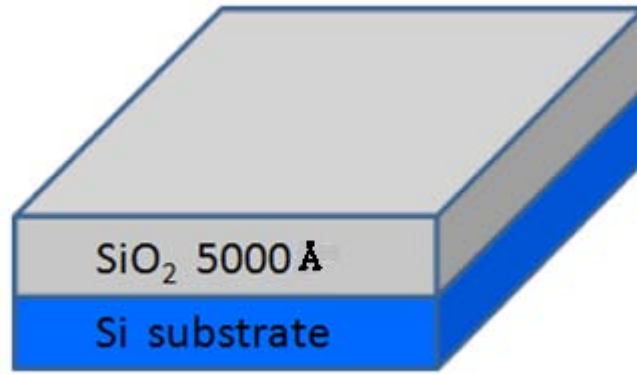


Fig. 2-1. SiO₂ layer is grown 5000Å on the Si substrate.

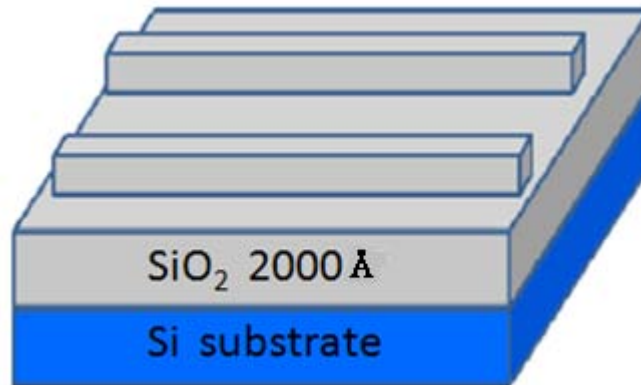


Fig. 2-2. Etching SiO₂, and the height is about 3000Å.

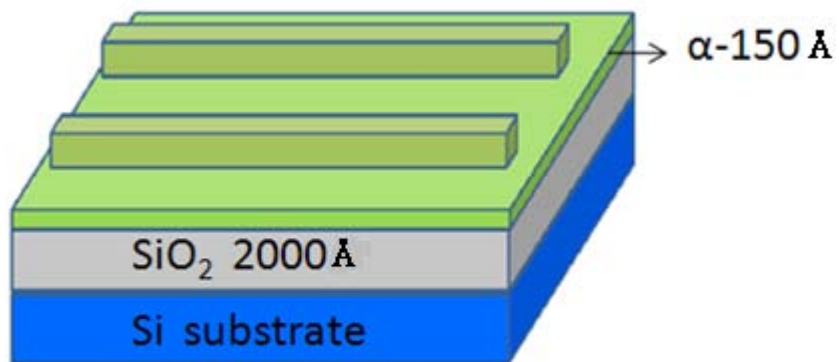


Fig. 2-3. Depositing α - Si 150Å on the SiO₂ layer.

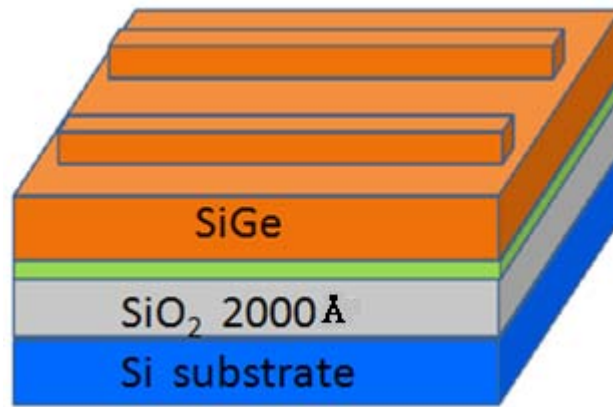


Fig. 2-4. Depositing SiGe layer on the amorphous Si layer.

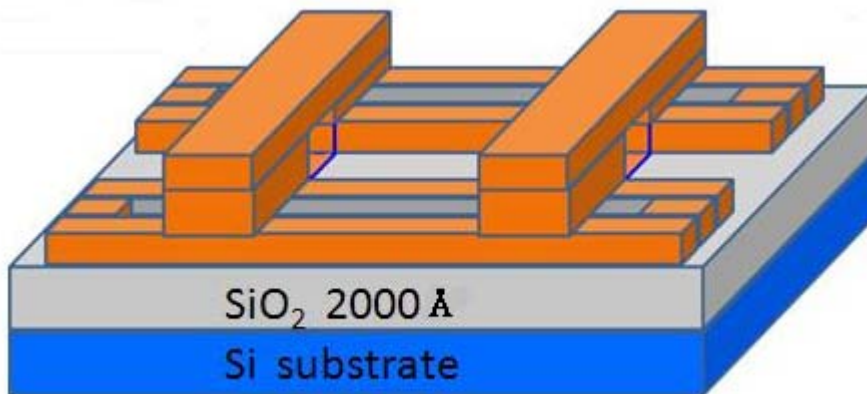


Fig. 2-5. Defined nanowire and S/D.

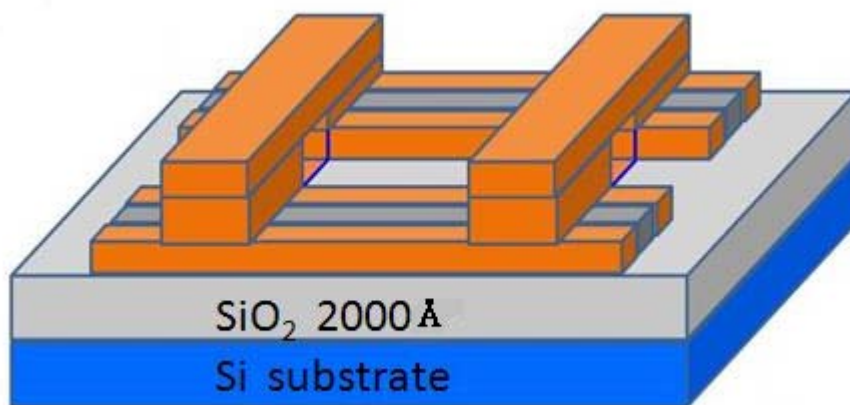


Fig. 2-6. Etching two side parallel nanowires.

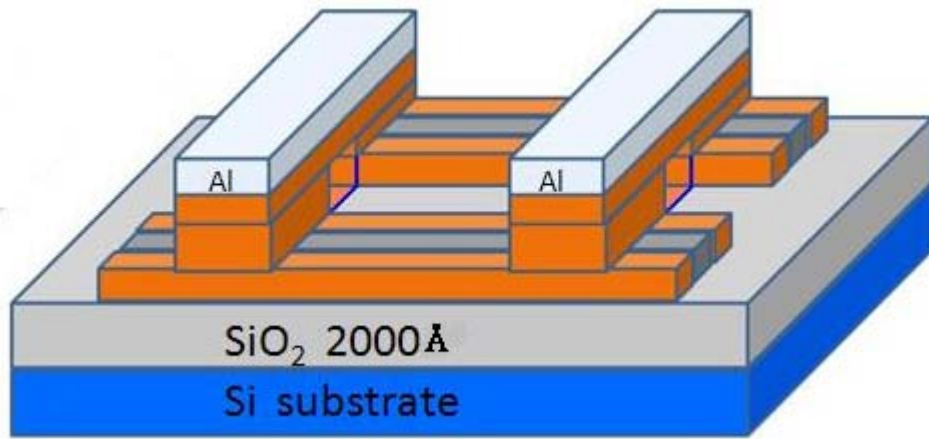


Fig. 2-7. Defined Al contact pad.

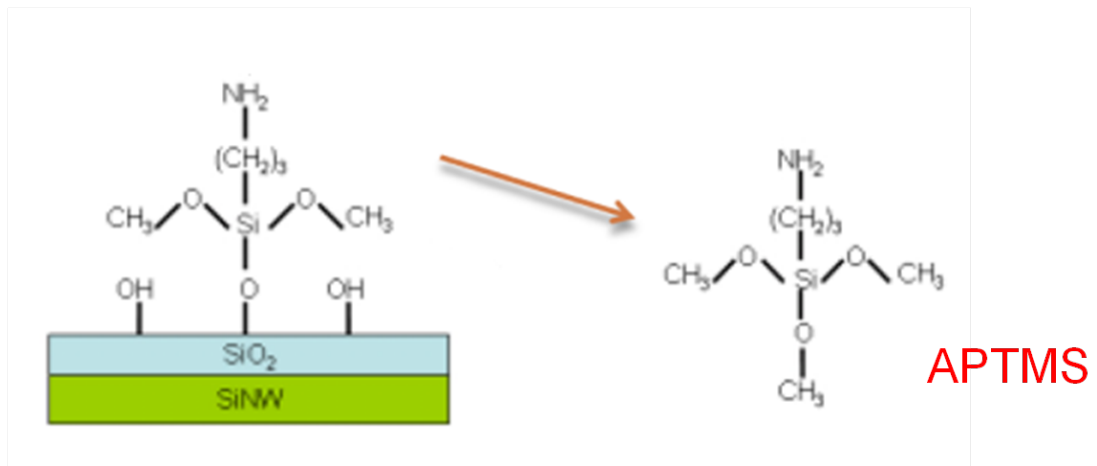


Fig. 2-8. APTMS binds silicon oxide layer.

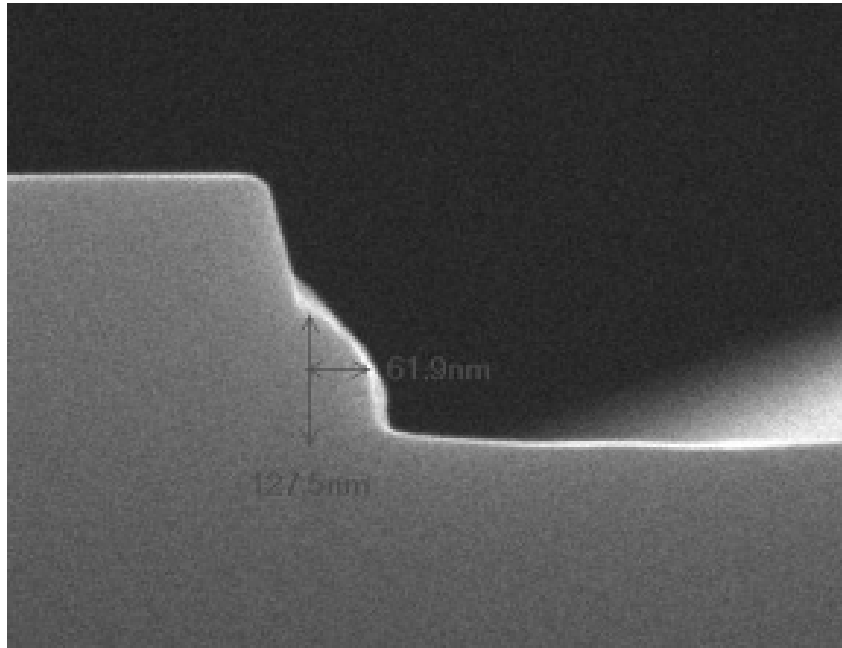


Fig. 3-1. SEM image of Si₉₃Ge₇ nanowire.

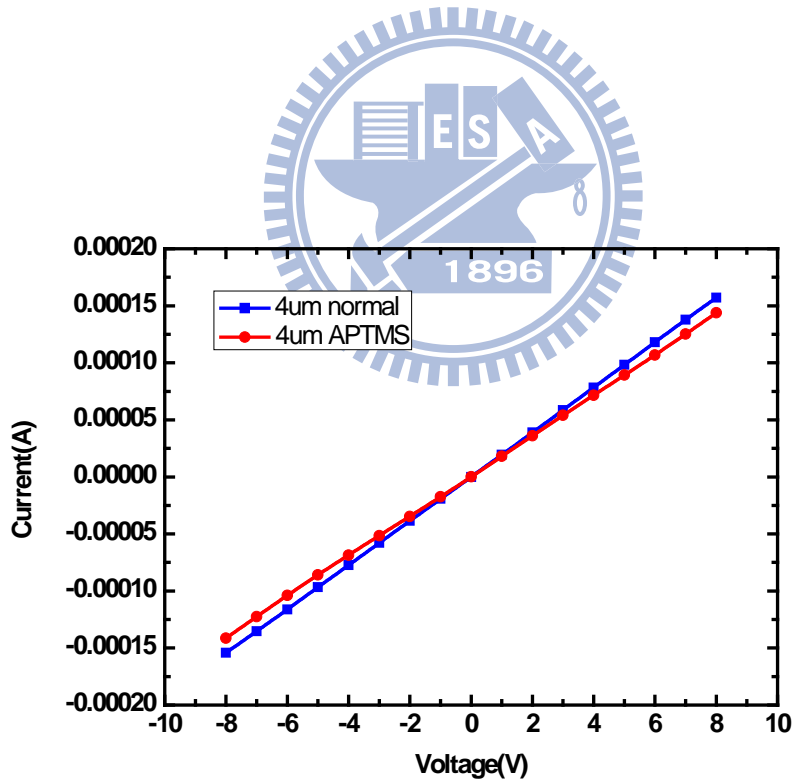


Fig. 3-2. I_D - V_D curve of Si₉₃Ge₇ nanowire which is 4 μ m long before and after dipped APTMS.

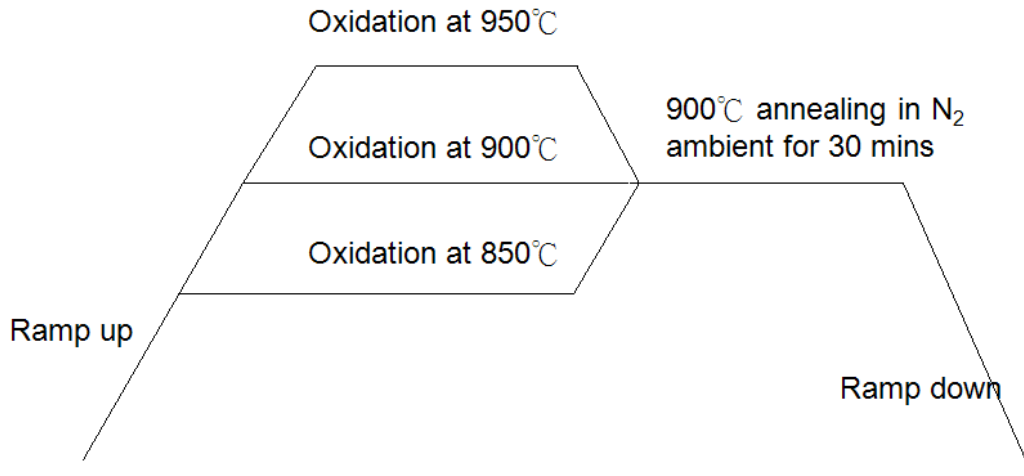


Fig. 3-3. Process of forming non-homogeneous SiGe nanowire with three different temperature and post-annealing at 900°C in N₂ ambient for 30 minutes.

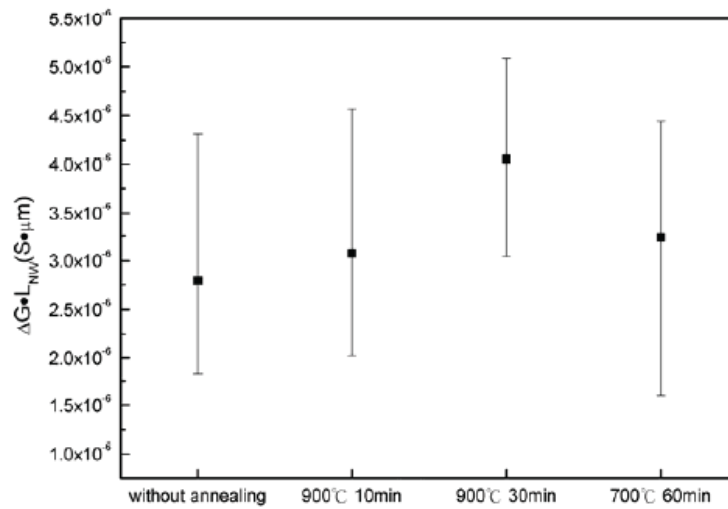


Fig. 3-4. Annealing conditions after oxidation (After C.H.T. et al, Ref. [24]).

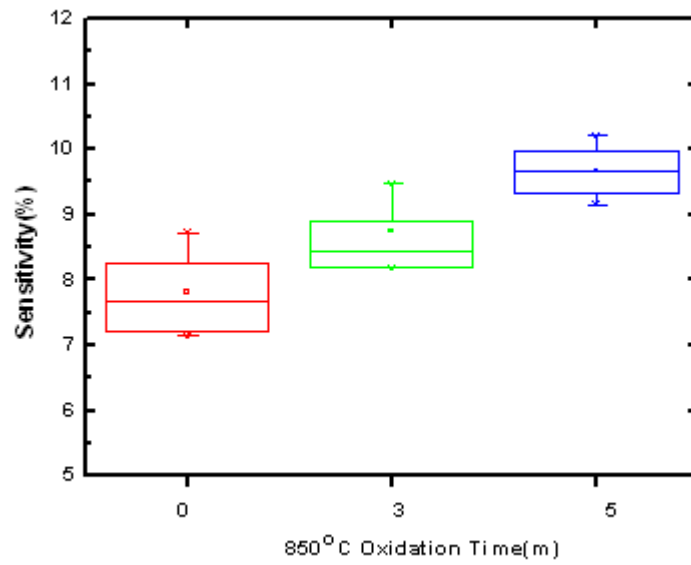


Fig. 3-5. Sensitivity distribution of oxidation at 850°C with different time.

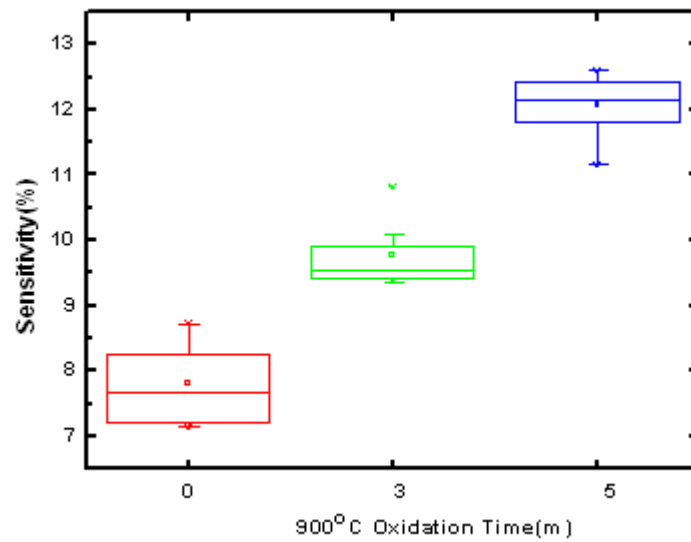


Fig. 3-6. Sensitivity distribution of oxidation at 900°C with different time.

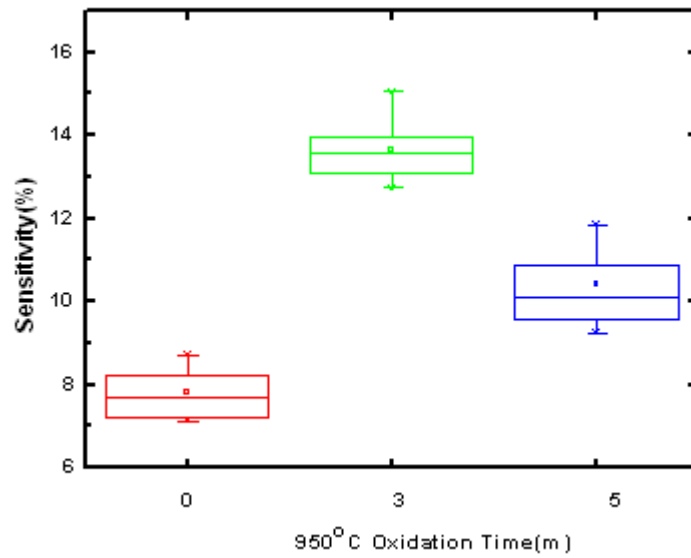


Fig. 3-7. Sensitivity distribution of oxidation at 950°C with different time.

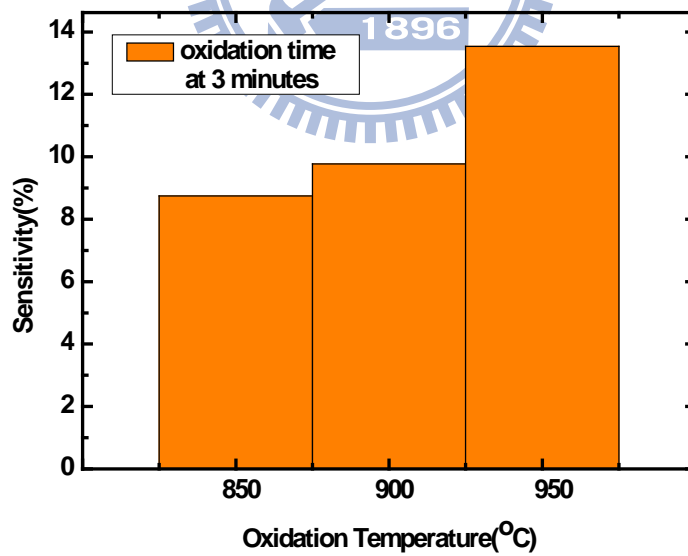


Fig. 3-8. Sensitivity distribution of oxidation time fixed 3 minutes with different oxidation temperatures.

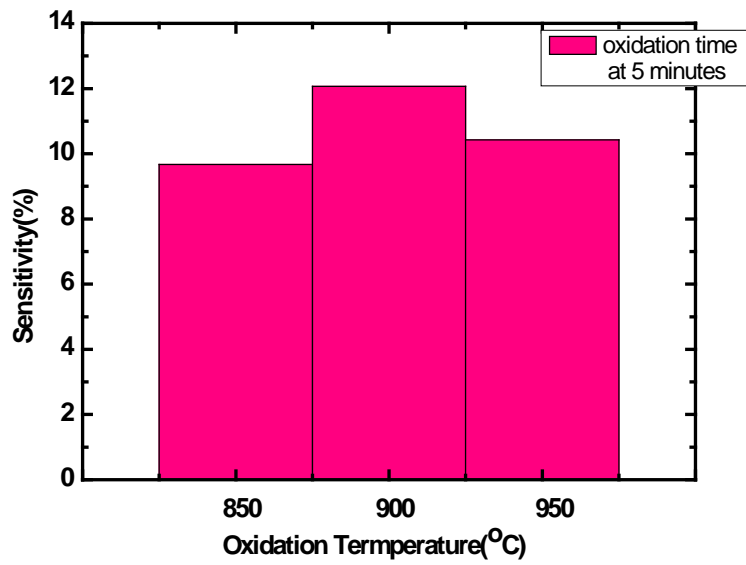


Fig. 3-9. Sensitivity distribution of oxidation time fixed 5 minutes with different oxidation temperatures.

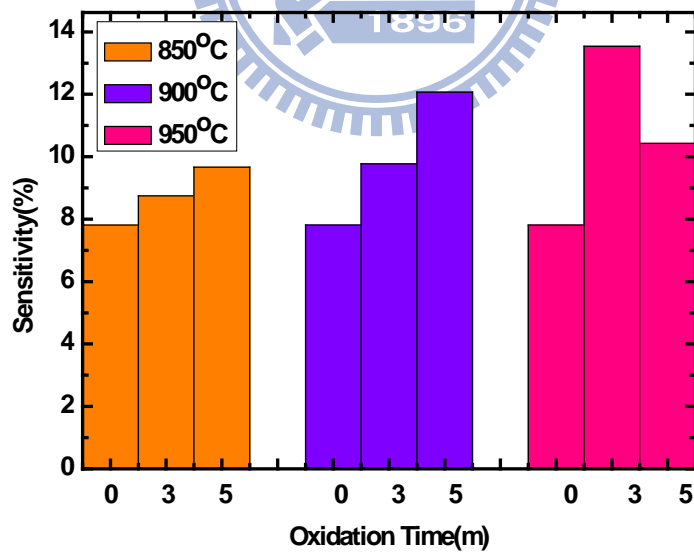


Fig. 3-10. A bar chart of sensitivity distribution with different conditions.

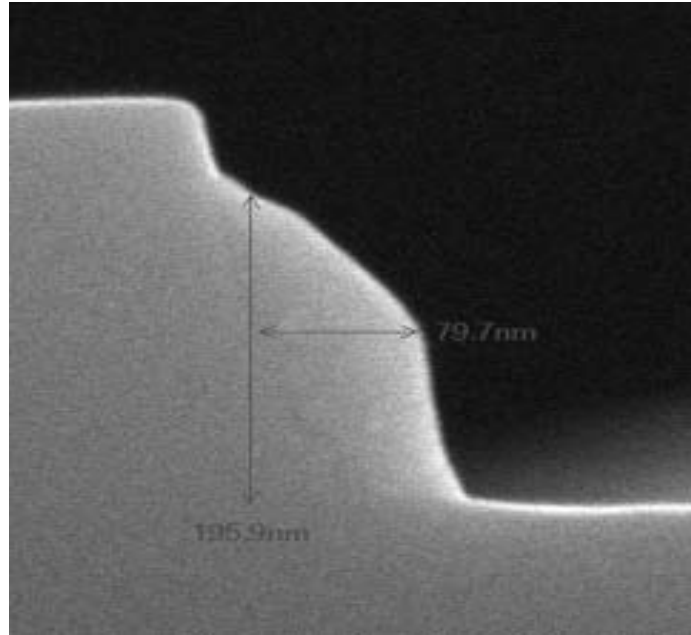


Fig. 4-1. SEM of Si₈₆Ge₁₄ nanowire.

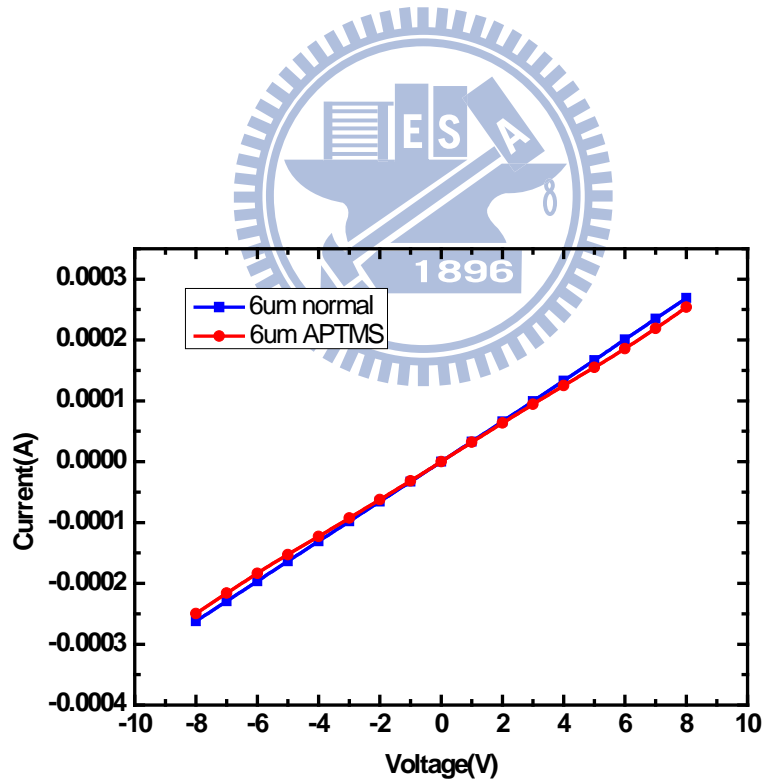


Fig. 4-2. I_D-V_D curve of Si₈₆Ge₁₄ nanowire which is 6um long before and after dipped APTMS.

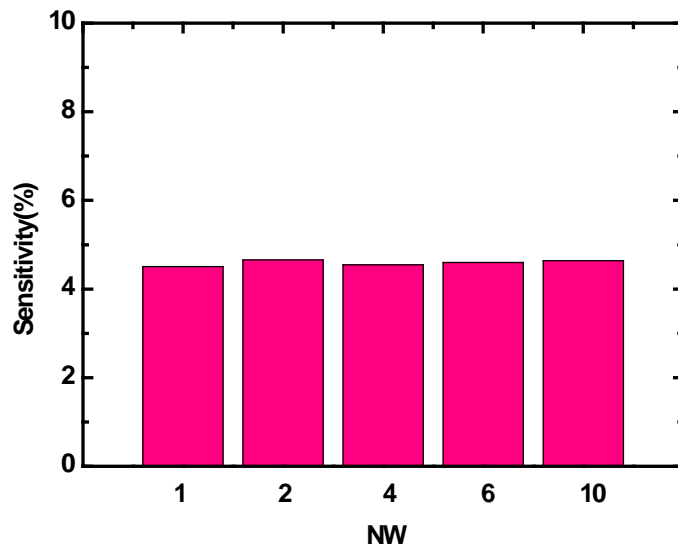


Fig. 4-3. Average sensitivity distribution with different parallel connection number of nanowire.

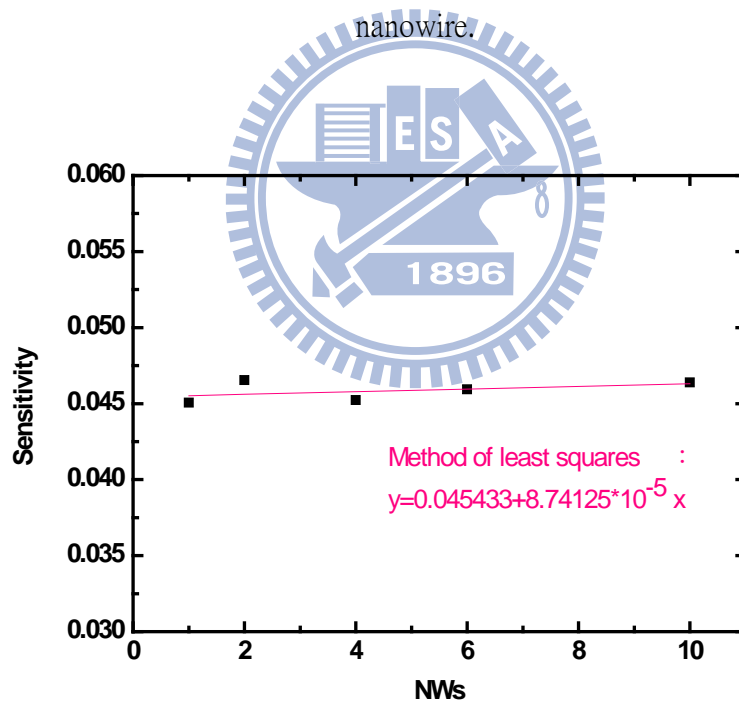


Fig. 4-4. Method of least squares of average sensitivity.

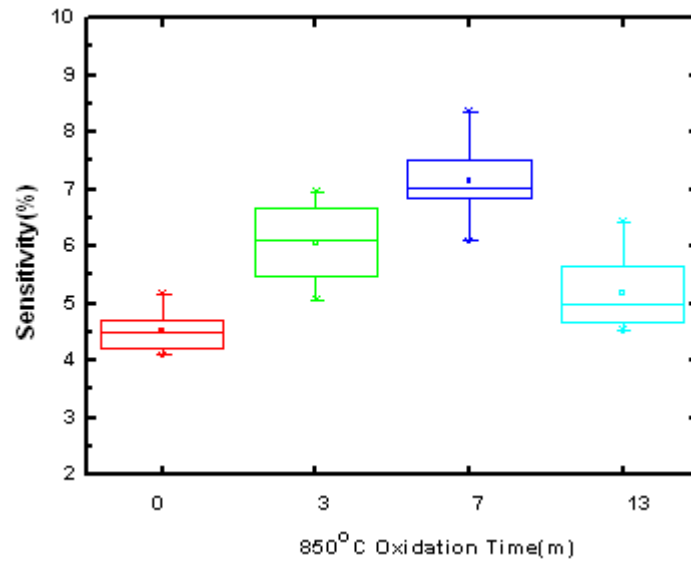


Fig. 4-5. Sensitivity distribution of oxidation at 850°C with different time.

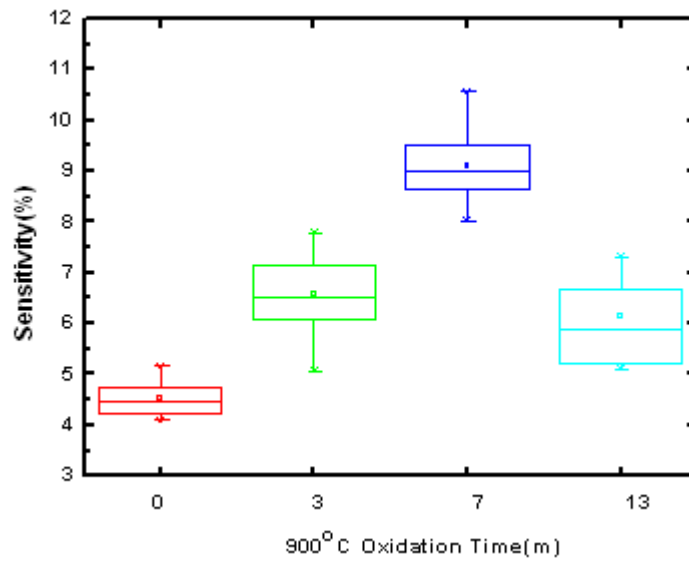


Fig. 4-6. Sensitivity distribution of oxidation at 900°C with different time.

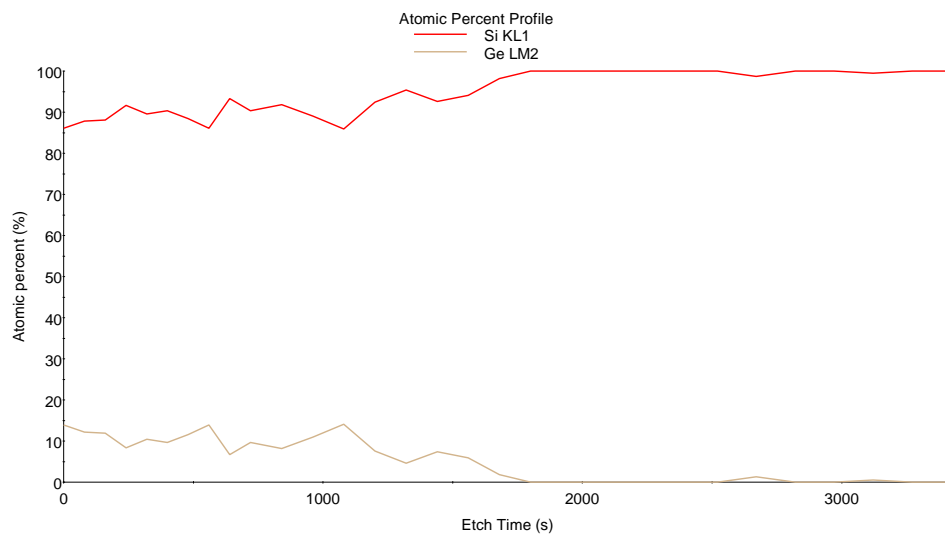


Fig. 4-7. Auger analysis of Si₈₆Ge₁₄ nanowire without oxidation.

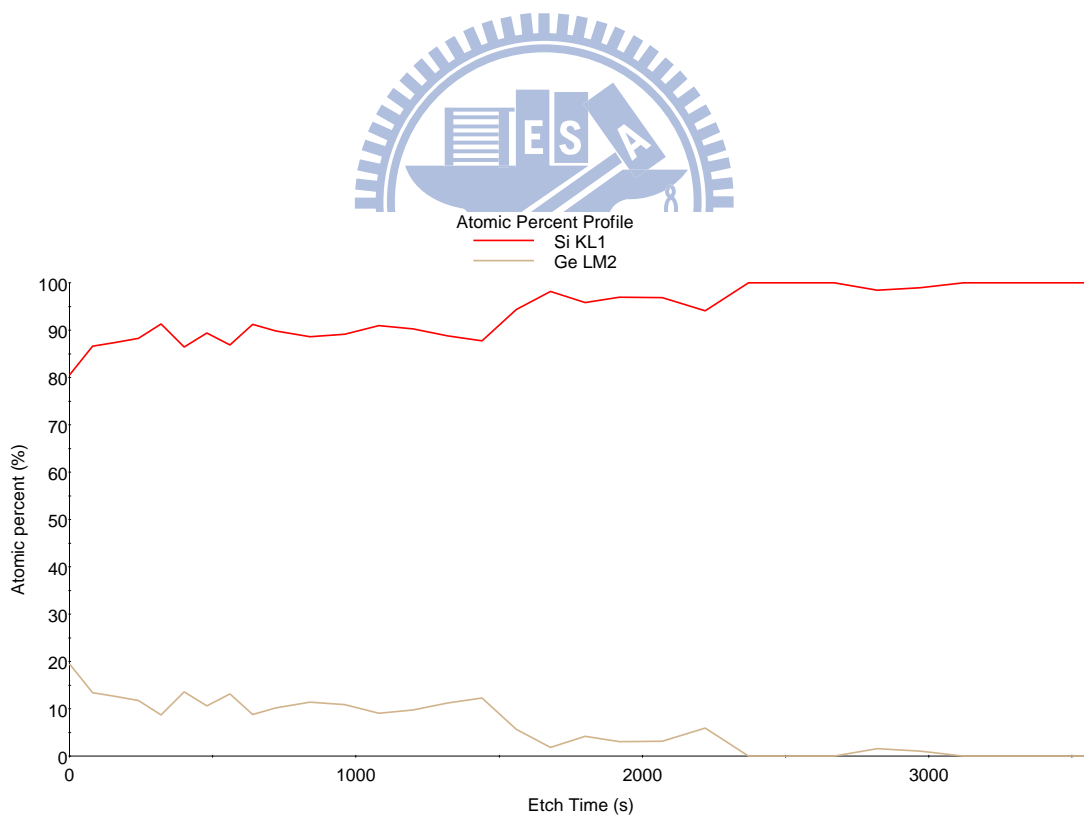


Fig. 4-8. Auger analysis of Si₈₆Ge₁₄ nanowire at oxidation temperature 900°C for 7 minutes.

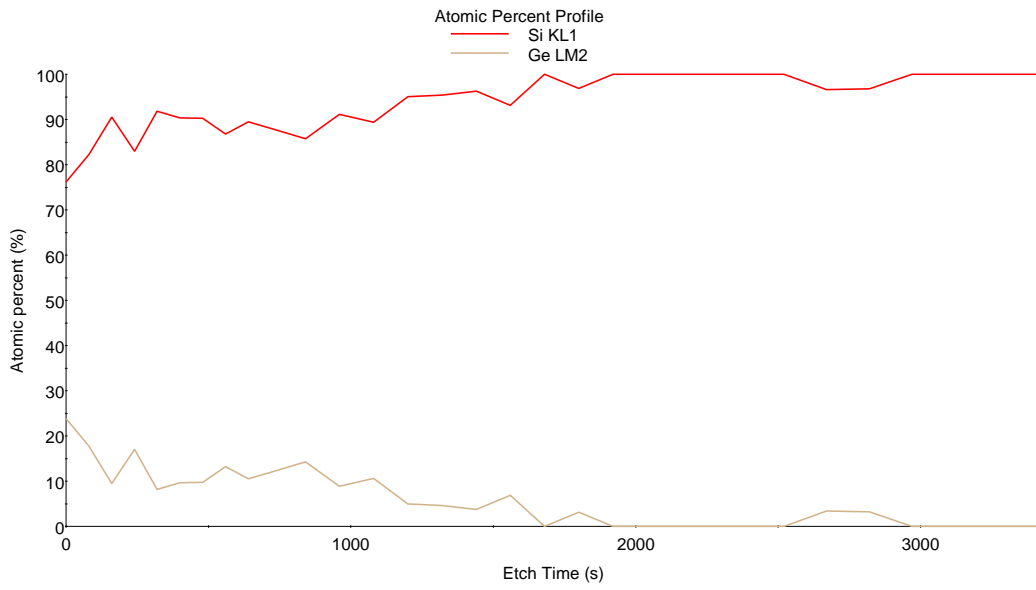


Fig. 4-9. Auger analysis of Si₈Ge₁₄ nanowire at oxidation temperature 900°C for 13 minutes.

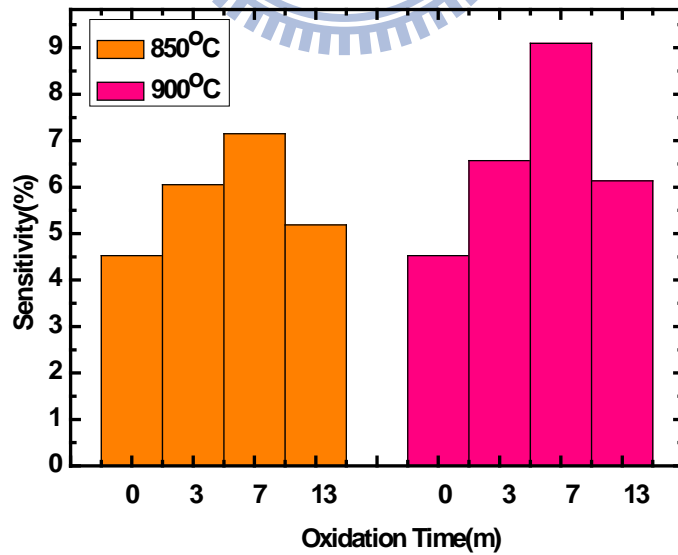


Fig. 4-10. A bar chart of sensitivity distribution with different conditions.

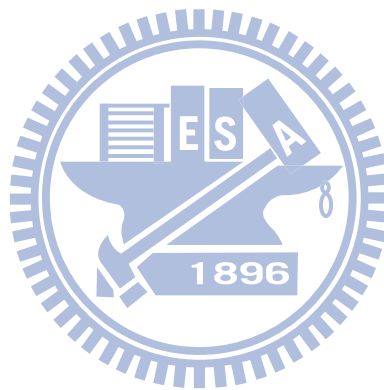
References :

- [1] Yi Cui, Qingqiao Wei, Hongkun Park, Charles M. Lieber, “Nanowire Nanosensors for Highly Sensitive and Selective Detection of Biological and Chemical Species,” *Science*, vol. 293, no. 5533, pp. 1289-1292, August 17, 2001.
- [2] Z.Li, Y. Chen, X. Li, T. I. Kamins, K. Nauka, and R. S. Williams, “Sequence-Specific Label-Free DNA Sensors Based on Silicon Nanowires,” *NANO LETTERS* vol. 4, no. 2, pp. 245-247, 2004.
- [3] Fernando Patolsky, Gengfeng Zheng, Oliver Hayden, Melike Lakadamyali, Xiaowei Zhuang, “Electrical detection of single viruses,” *PNAS*, vol. 101, no. 39, PP. 14017-14022, September 28, 2004.
- [4] E.Comini, G.Faglia, and G. Sberveglieri, “Stable and highly sensitive gas sensors based on semiconducting oxide nanobelts,” *APPLIED PHYSICS LETTERS*, vol. 81, no. 10, pp. 1869-1871, September 2, 2002.
- [5] Chao Li, Daihua Zhang, Xiaolei Liu, Song Han, Tao Tang, Jie Han, and Chongwu Zhou, “In₂O₃ nanowires as chemical sensors,” *APPLIED PHYSICS LETTERS*, vol. 82, no. 10, pp. 1613-1615, March 10, 2003.
- [6] Haiqing Liu, Jun Kameoka, David A. Czaplewski, and H. G. Craighead, “Polymeric Nanowire Chemical Sensor,” *Nano Letters*, vol. 4, no. 4, pp. 671-675, 2004.
- [7] Yufeng Ma, Jianming Zhang, Guojin Zhang, and Huixin He, “Polyaniline Nanowires on Si Surface Fabricated with DNA Templates,” *American Chemical Society*, vol. 126, pp. 7097-7101, 2004.
- [8] Kyun Tae Kim, Sang Jun Sim, and Sung Min Cho, “Hydrogen Gas Sensor Using Pd Nanowires Electro-Deposited Into Anodized Alumina Template,” *IEEE Sensors Journal*, vol. 6, no. 3, pp. 509-513, June, 2006.

- [9] Fredic Favier, Erich C. Walter, MichealP.Zach, Thorsten Benter, and Reginald M.Penner, "Hydrogen Sensors and Switches from Electrodeposited Palladium Mesowire Arrays," *Science*, vol. 293, no. 5538, pp. 2227-2231, September, 2001.
- [10] R.S. Wagner and W. C. Ellis, Bell Telephone Laboratories, Inc. , Murray Hill, New Jersey, "VAPOR-LIQUID-SOLID MECHANISM OF SINGLE CRYSTAL GROWTH," *APPLIED PHYSICS LETTERS*, vol. 4, no. 5, pp. 89-90, March 1, 1964.
- [11] S.J.Whang, S. J. Lee, W. F. Yang, and B. J. Cho, D. L. Kwong, "Study on the synthesis of high quality single crystalline $\text{Si}_{1-x}\text{Ge}_x$ nanowire and its transport properties," *APPLIED PHYSICS LETTERS* vol. 91, no. 072105, pp. 1-3, 2007.
- [12] Sung Dae Suk, Kyoung Hwan Yeo, Keun Hwi Cho, Ming Li, Yun Young Yeoh, Sung-Young Lee, Sung Min Kim, Eun Jung Yoon, Min Sang Kim, Chang Woo Oh, Sung Hwan Kim, Dong-Won Kim, and Donggum Park, "High-Performance Twin Silicon Nanowire MOSFET (TSNWFET) on Bulk Si Wafer," *IEEE TRANSACTIONS ON NANOTECHNOLOGY*, vol. 7, no. 2, pp. 181-184, March, 2008.
- [13] Gengfeng Zheng, Fernando Patolsky, Yi Cui, Wayne U Wang&Charles M Lieber, "Multiplexed electrical detection of cancer markers with nanowires sensor arrays," *NATURE BIOTECHNOLOGY*, vol. 23, no. 10, pp. 1294-1301, October, 2005.
- [14] Alexandra C. Ford, Johnny C. Ho, Yu-Lun Chueh, Yu-Chih Tseng, Zhiyong Fan, Jing Guo, Jeffrey Bokor, and Ali Javey, "Diameter-Dependent Electron Mobility of InAs Nanowires," *NANO LETTERS*, vol. 9, no. 1, pp. 360-365, 2009.
- [15] Ryan Tu, Li Zhang, Yoshio Nishi, and Hongjie Dai, "Measurement the Capacitance of individual Semiconductor Nanowires for Carrier Mobility Assessment," *NANO LETTERS*, vol. 7, no. 6, pp. 1561-1565, 2007.

- [16] Mached I. van der Meulen, Nikolay Petkov, Michael A. Morris, Olga Kazakova, Xinhai Han, Kang L. Wang, Ajey P. Jacob, and Justin D. Holmes, "Single Crystalline Ge_{1-x}Mn_x Nanowires as Building Blocks for Nanoelectronics," *NANO LETTERS*, vol. 9, no. 1, pp. 50-56, 2009.
- [17] D. Wang, H. DAI, "Germanium nanowires: from synthesis, surface chemistry, and assembly to devices," *Applied Physics A Materials science & Processing*, 85, pp. 217-225, 2006.
- [18] Dunwei Wang, Qian Wang, Ali Javey, Ryan Tu, and Hongjie Dai, "Germanium nanowire field-effect transistors with SiO₂ and high- κ HfO₂ gate dielectrics," *APPLIED PHYSICS LETTERS*, vol. 83, no. 12, pp. 2432-2434, September 22, 2003.
- [19] Fernando Patolsky, Gengfeng Zheng & Charles M Lieber, "Nanowire sensors for medicine and the life sciences," *Nanomedicine*, vol. 1, pp. 51-65, June, 2006.
- [20] Pradeep R. Nair, and Muhammad A. Alam, "Design Considerations of Silicon Nanowire Biosensors," *IEEE TRANSACTIONS ON ELECTRON DEVICES*, vol. 54, no. 12, pp. 3400-3408, December, 2007.
- [21] Yee-Chia Yeo, Qiang Lu, Tsu-Jae King, Chenming Hu, Takayuki Kawashima, Masato Qishi, Supika Mashiro, and Junro Sakai, "Enhanced Performance in Sub-100nm CMOSFETs Using Strained Epitaxial Silicon-Germanium," *IEDM*, pp. 753, 2000.
- [22] T. Tezuka, N. Sugiyama, and S. Takagi, "Fabrication of strained Si on an ultrathin SiGe-on-insulator virtual substrate with a high-Ge fraction," *APPLIED PHYSICS LETTERS*, vol. 79, no. 12, pp. 1798-1800, SEPTEMBER 17, 2001.

- [23] P.E. Hellberg, S. L. Zhang, F. M. d' Heurle *et al.*, “Oxidation of silicon—germanium alloys. II. A mathematical model,” *Journal of Applied Physics*, vol. 82, no. 11, pp. 5779-5787, 1997.
- [24] Chu-Hsiang Teng, “Novel Application of Non-homogeneous SiGe Nanowire for Highly Sensitive Biosensor,” Thesis of Department of Electronics Engineering&Institute of Electronics College of Electrical. Hsinchu, National Chiao Tung university, pp. 68, Fig. 4-8, 2008.



簡 歷

姓 名：鄭文魁

性 別：男

出生日期：民國 74 年 5 月 16 日

出生地：台灣省台南縣

住址：台南縣新營市周武街 79 巷 22 弄 1 號

學歷：興國高級中學 (民國 89 年 9 月~民國 92 年 6 月)

國立高雄大學電機工程學系 (民國 92 年 9 月~民國 96 年 6 月)

國立交通大學電子工程所 (民國 96 年 9 月~民國 98 年 9 月)

碩士論文：應用非均勻矽鍺奈米線在生物感測器上提升其靈敏度

Utilizing Non-Homogeneous SiGe Nanowires to Enhance Sensitivity

Obviously in Biosensor

